Surface Complexation at
the Iron Oxide/Water Interface

Experimental Investigations and Theoretical Developments

Magnus Gunnarsson

Akademisk avhandling

Surface Complexation at the Iron Oxide/Water Interface;
Experimental Investigations and Theoretical Developments

Cover: Schematic picture of a charged spherical hematite (α-Fe_2O_3) particle suspended in an electrolyte solution. The blue diffuse area around the particle represents the screening atmosphere.

Abstract

The properties of the iron oxide/water interface are of utmost importance for the chemistry in natural aquatic environments as well as for processes related to the corrosion of metals. In these kinds of systems iron oxides are present as small particles precipitated on surfaces or suspended in solution. Inherent features of the iron oxide surface are for example the tendency to build up a surface charge and its capacity of sorbing various ionic species. These things and other related phenomena can be studied using the concept of surface complexation.

This thesis contains both experimental and theoretical surface complexation studies of the iron oxide/water interface. Colloidal particles of hematite (α-Fe$_2$O$_3$) and goethite (α-FeOOH) have been prepared on lab scale and used as model substances in the experimental investigations. The charging properties of the suspended particles have been studied using potentiometric titration. In addition, the electroacoustic technique has been used to study the particles under the influence of a high frequency electric field. With this technique the so-called zeta-potential and the size of the suspended particles can be determined. Most of the experimental data were described satisfactorily using a 1-pK basic Stern surface complexation model. For the hematite particles in NaNO$_3$ solution it was necessary to account for ion pairing of electrolyte ions into the Stern plane.

Besides using existing surface complexation models a reformulation of the underlying theory has been performed using statistical mechanics. In this way a molecular description of surface complexation was obtained and with the new model it was possible to go one step beyond the equilibrium constants and the Gouy-Chapmann theory presently used in surface complexation. Included are descriptions of particle screening and specific binding of protons at surface sites. To account also for nonlinear electrostatic response a layer of condensed counterions was introduced. The new model was applied to titrated surface charge data of goethite at various background concentrations and a good agreement between the experimental data and the model was obtained. Both the size of the screening ions and the central particle size were shown to be of importance for the surface charge.

Because of its relevance in the nuclear power industry the sorption of cobalt(II) on hematite was also studied. Sorption data obtained from radioactive tracer measurements was combined with data from potentiometric titrations. This combination yielded valuable information on the pH dependence of both the amounts of cobalt sorbed on the surface and the number of protons released as a consequence of the sorption. The cobalt sorption was modelled with the 1-pK basic Stern model. By introducing a low concentration of high affinity surface sites for cobalt sorption it was possible to describe the sorption in very wide interval of cobalt concentrations, ranging from 10^{-8} M to 10^{-4} M. A simplified version of the model for cobalt sorption was used as a part of the interpretation of online radioactivity data from nuclear boiling water reactors.

Keywords: colloidal particles, potentiometric titration, surface charge, cobalt sorption, activity build-up, 1-pK basic Stern model, electrokinetics, electroacoustics, zeta-potential, site binding, statistical mechanics, corrected Debye-Hückel theory.

Included papers

This thesis is based on the studies presented in the following papers, referred to in the text by their Roman numerals:

I. Sorption Studies of Cobalt(II) on Colloidal Hematite Using Potentiometry and Radioactive Tracer Technique
    Magnus Gunnarsson, Anna-Maria Jacobsson, Stefan Ekberg, Yngve Albinsson and Elisabet Ahlberg
    J. Colloid Interface Sci. 231, 326-336 (2000)

II. Electroacoustic and Potentiometric Studies of the Hematite/Water Interface
    Magnus Gunnarsson, Mikael Rasmusson, Staffan Wall, Elisabet Ahlberg and Jonathan Ennis
    J. Colloid Interface Sci. 240, 448-458 (2001)

III. Application of the "Parsons-Zobel plot" in Surface Complexation Modelling of the Metal (Hydr)oxide/Water Interface
    Magnus Gunnarsson and Elisabet Ahlberg
    Manuscript

IV. Corrected Debye-Hückel Analysis of Surface Complexation – I. Bulk Salt Limit
    Zareen Abbas, Magnus Gunnarsson, Elisabet Ahlberg and Sture Nordholm
    J. Colloid Interface Sci. 243, 11-30 (2001)

V. Corrected Debye-Hückel Analysis of Surface Complexation – II. A Theory of Surface Charging
    Magnus Gunnarsson, Zareen Abbas, Elisabet Ahlberg, Sylvia Gobom and Sture Nordholm
    J. Colloid Interface Sci. 249, 52-61 (2002)

VI. Corrected Debye-Hückel Analysis of Surface Complexation – III. Spherical Particle Charging Including Ion Condensation
    Magnus Gunnarsson, Zareen Abbas, Elisabet Ahlberg and Sture Nordholm
    Submitted to *Langmuir*

Related work not included as appended papers:

Corrected Debye-Hückel Theory of Salt Solutions - Size Asymmetry and Effective Diameters
Zareen Abbas, Magnus Gunnarsson, Elisabet Ahlberg and Sture Nordholm
J. Phys. Chem. B. 106, 1403-1420 (2002)

A new model for activity buildup in BWRs adopting theories for surface complexes and diffusion in oxide layers
Klas Lundgren, Tormod Kelén, Magnus Gunnarsson and Elisabet Ahlberg
SSI Project Report P 1203.00 (2001)

Contents

Chapter 1

Introduction

Mineral oxides are widespread in nature and are often present as suspended particles in aquatic environments. To a large extent, the chemical processes in natural waters are determined by the surface properties of these small particles. In many cases chemical reactions at a surface lead to an accumulation of matter at the interface. A common term for such a process is sorption. One type of surface that is of both practical and fundamental interest is the iron oxide surface. Due to the high sorption capacity of iron oxide particles they are responsible for many transport mechanisms of trace metals and radioactive isotopes in natural aqueous systems.

The surface properties of iron oxides are also very important for the understanding of various processes related to the corrosion of metals. Both the subsequent growth and the inherent features of the corrosion products will be determined by the conditions at the metal oxide/water interface. Actually, this work has been initiated due to a phenomenon observed in nuclear boiling water reactors. Metallic surfaces covered by films and/or particles of various metal oxides tend to sorb radioactive ionic species from the water. This leads to a build up of radioactivity on these surfaces. It is an unwanted effect since it contributes to the total radiation dose levels in the reactor. A better chemical and physical understanding of the properties of the metal oxide/water interface will facilitate the construction of sound models for this kind of processes. Such models can then be used to predict properties at new conditions and may also be a valuable tool for preventing unwanted effects, in this case the activity build up in nuclear reactors.

1.1 Surface complexation

One fundamental property of the metal oxide surface is its tendency to build up a surface charge when in contact with water. That will induce electrostatic effects in the neighbourhood of the charged particle. The surface charge is therefore a very important parameter with respect to many features of the dispersed materials. For example it will affect the colloidal stability and the capacity of sorbing different ionic species from the aqueous phase onto the surface.

In surface complexation theory the sorption reactions are described in terms of chemical reactions between surface functional groups (sites) and dissolved chemical species. To account also for the electrostatic effects mentioned above a description of the solution outside a charged surface has to be included. The first

surface complexation models were developed about 30 years ago [1-3]. Since then, a huge number of publications have been devoted to develop more or less sophisticated models so that experimental data can be very well described. However, the fundamental concepts upon which all surface complexation models are based have remained almost the same. Dzombak and Morel [4] summarized the concept as follows:

1. Sorption on oxides takes place at specific coordination surface sites in a manner analogous to complexation reactions in solution.
2. The sorption reactions can be described quantitatively by mass law equations.
3. Surface charge results from the sorption reactions themselves.
4. The effect of surface charge on sorption can be taken into account by applying a correction factor derived from the electric double layer theory to mass law (equilibrium) constants for surface reactions.

In the present work we have used the surface complexation concept as it is described above to interpret various phenomenon and experimental data of the iron oxide/water interface. However, we have also challenged the concept to some extent by reformulating a surface complexation theory based on statistical mechanics. In that approach some of the points above have been replaced by a molecular description of the processes at the oxide/liquid interface.

1.2 Scope and outline of this thesis

The work presented in this thesis is of both experimental and theoretical character. Furthermore, it contains parts of fundamental research as well as work of more applied nature. The main experimental techniques are presented in chapter 2. Features of the iron oxide/liquid interface are described in more detail in chapter 3. It contains a background to the surface complexation concept but also various experimental results describing the charging process of the iron oxide surface. In chapter 4 the statistical mechanical approach to surface complexation is outlined. Here, model calculations are compared mainly to surface charge data of suspended goethite (α-FeOOH) particles. Because of its relevance in the nuclear power industry the sorption of cobalt on hematite (α-Fe$_2$O$_3$) has been studied. The results and a proposed surface complexation model are discussed in chapter 5. A simplified version of the model for cobalt sorption was used as a part of the interpretation of online radioactivity data from boiling water reactors. This is described in chapter 6. Finally, some concluding remarks are given in chapter 7.

Chapter 2

Experimental

2.1 Preparation and characterisation of hematite and goethite

Hematite (α-Fe_2O_3) is, together with goethite (α-FeOOH), one of the most frequently studied iron oxides in aqueous media. Both of them are very stable oxides at ambient temperatures. They have well defined crystal structures and are often the end products of many transformations in nature. They are therefore very important for the different transport mechanisms of for example trace elements and radioactive isotopes. Hematite can also be formed during corrosion of metals at elevated temperatures and is therefore suitable as a model for corrosion products. Therefore colloidal hematite and goethite have been chosen in this work as model substances for the examination of the oxide/liquid interface.

The hematite particles were prepared by forced hydrolyses of acidified and diluted $FeCl_3$ solutions. The shape and size of the particles are strongly dependent on storage time and temperature, $FeCl_3$ concentration and pH [5]. A procedure similar to that reported by Matijevic´ [6] was used. The details are given in Paper I and II. Particle size and shape were studied with scanning electron microscopy (SEM). In Fig. 2.1 two different sets of particles are shown. These particles were prepared from solutions with different $FeCl_3$ concentration, which clearly affected the shape and the size.

a   b
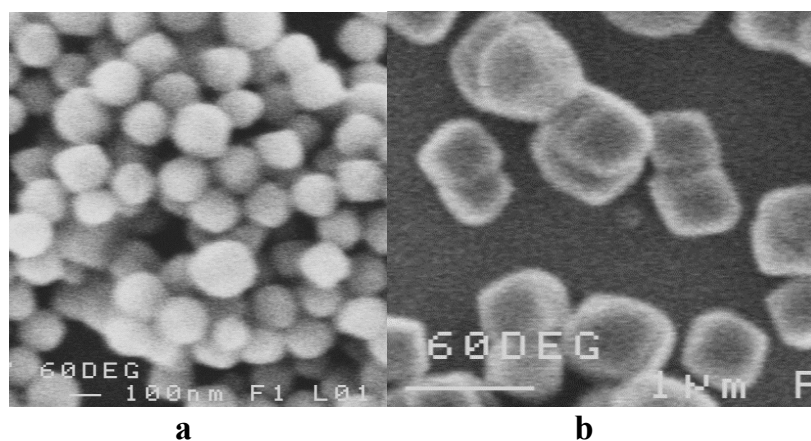
Figure 2.1   SEM images of colloidal hematite particles synthesised and studied in this work.
a) Nearly spherical particles with a diameter of ~0.1 µm, prepared from a solution containing 0.02 M $FeCl_3$ and 1 mM HNO_3, stored at 100 °C for 24 h.
b) Particles with a diameter of ~0.6 µm, prepared from a solution containing 0.04 M $FeCl_3$ and 1 mM HNO_3, stored at 100 °C for 7 days.
Pictures reprinted from Paper I and II.

The goethite particles were prepared by mixing solutions of $Fe(NO_3)_3$ and KOH according to the method by Atkinson *et al.* [7]. The suspension formed was washed repeatedly by gravitational sedimentation and subsequent removal of the supernatant. Both the hematite and the goethite samples were studied by X-ray diffraction analysis to verify the crystal structure. To measure the surface area of the products the BET nitrogen adsorption technique was used. This is an *ex situ* technique where the colloidal particles are first dried and subsequently degassed. It is not obvious that this yields a result representative for the surface area in suspension. Therefore, the particle surface area has also been extracted from experimental surface charge data. A description of the procedure and some results are given in section 3.2.

2.2 Potentiometric titrations

Potentiometric titration is in principle a rather simple standard experiment. One only (!) has to measure pH in a solution/suspension during subsequent additions of acid or base. It is then possible from stoichiometric calculations to draw conclusions about the reactions that have taken place. In this work it is the surface reactions that are of interest and therefore titrations of solutions containing colloidal hematite and goethite particles have been performed. In practice potentiometric titrations can be very time consuming and there are a lot of experimental details that can affect the data obtained. In addition, there are many different ways to perform the calculations and the analysis of the results. A detailed description of how the experiments have been performed and how the data have been analysed is therefore a prerequisite for reliable results from potentiometric titrations. Titrations of colloidal hematite are described in Paper I and II and of goethite in Paper IV.

If there are no other ions than protons and hydroxide ions that regulate the surface charge on the particles, potentiometric titrations can be used to obtain the primary surface charge density σ_o. The difference between the measured free proton concentration and the total proton concentration known from the additions of acid or base is used to calculate σ_o:

$$\sigma_o = \frac{F(n_{H^+} - n_{OH^-})}{S_A C_S V},$$ \hfill (2.1)

where F is the Faraday constant, n_i is the amount of adsorbed ion of type i in moles, S_A is the surface area in m^2g^{-1}, C_S is the hematite concentration in gl^{-1} and V is the volume of the suspension before the first addition from the burette. The magnitudes of n_{H^+} and n_{OH^-} are determined from the measured free proton concentration, the additions of acid or base and the experimentally determined point of zero charge pH_{pzc}.

σ_o is the charge located exactly at the particle surface. Due to a pronounced screening of this charge by counterions from the electrolyte the electrostatic potential will drop rapidly close to the surface. Some of the screening ions may be so strongly attached to the surface that they will follow the particle when it moves in the solution. To study these and related phenomena electrokinetics is very useful. One electrokinetic technique that has been used in this work will be described in the following section.

2.3 Electroacoustic measurements

Generally, an electrokinetic phenomenon occurs when an external field acts on a colloidal system. When a particle moves in an electrolyte solution a thin liquid layer will move with the particle. The layer between the moving and stationary liquid defines the slip plane and the potential in that plane is known as the electrokinetic potential or the ζ-potential.

One of the most familiar techniques in the area is electrophoresis where the motion of colloidal particles is studied under the influence of a static electric field. The sign and magnitude of the surface charge will determine the movement of the particles. The point on the pH-scale where there is no movement is called the isoelectric point, IEP. If an alternating field is applied to a colloid, the particles will move back and forth and give rise to the electroacoustic effect [8]. This effect is utilised in the commercial instrument AcoustoSizer, with which particle sizes and ζ-potentials can be determined. In combination with potentiometry described above the AcoustoSizer has been used in this work to study the charging properties of colloidal hematite (Paper II).

The AcoustoSizer measures the electrokinetic sonic amplitude (ESA) generated when charged colloidal particles oscillate under the influence of an alternating high-frequency electric field. For dilute suspensions (particle volume fraction $\phi <$ 0.02), the ESA signal and the particle-average dynamic mobility $\langle \mu_d \rangle$ are related to each other according to [8]

$$ESA(\omega) = A(\omega, K)\phi \frac{\Delta\rho}{\rho}\langle \mu_d \rangle, \qquad (2.2)$$

where A is an instrumental factor dependent on both ω, the angular frequency, and K, the conductivity of the suspension. $\Delta\rho$ is the density of the particles minus the density of the solvent (ρ). From the mobility the ζ-potential can be calculated. Different ways to do this will be described together with the results in section 3.4.

A schematic drawing of the AcoustoSizer cell is shown in Fig. 2.2. The colloidal suspension is placed in the beaker (400 ml) in the middle. It contains a stirrer and probes for temperature, conductivity and pH measurements. Furthermore, there are four thermally conducting ceramic rods for temperature control. For simplicity these things has been omitted in the figure.
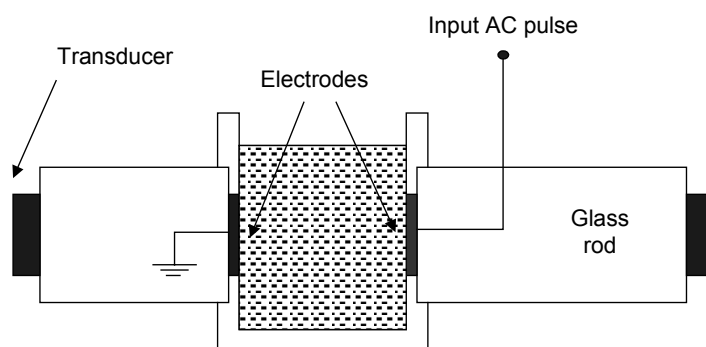
Figure 2.2 Schematic drawing of the AcoustoSizer cell.

A pulse of a high frequency field (varied between 0.3 and 11.15 MHz) is applied over the two parallel plate electrodes, which are in contact with the suspension. The resulting sound wave will move out in the glass rods on each side of the beaker. The pressure waves are then detected and converted to electrical signals by the transducers, consisting of piezoelectric crystals, at the end of the glass rods. It is the transducer on the right hand side in the figure that is used for measuring the ESA signal. The left glass rod and transducer is used to calibrate the acoustic impedance of the instrument. A more detailed description of the principles of the technique and the theory behind the electroacoustic effect can be found in Refs. [8, 9].

2.4 Cobalt(II) sorption studies

To study how the total amount of a specific chemical species (in this case Co(II)) is distributed between an aqueous and a solid phase sorption studies are very useful. The general route is to put the species of interest into the relevant chemical environment and then allow the chemical system to equilibrate. The solid and the aqueous phase are then separated and the amount of the species in the aqueous and/or solid phase can be measured. In Paper I, where we have studied cobalt(II) sorption on hematite a radioactive tracer technique has been used. The Department of Nuclear Chemistry at Chalmers University of Technology performed these measurements. The sorption of Co(II) was studied both as a function of pH and of cobalt concentration at constant ionic strength using the radioactive isotope ^{60}Co. For experimental details see Ref. [10] and Paper I.

To complement the information obtained from the radioactive tracer studies potentiometric titrations were also performed. From titrations done both with and without Co(II) in the hematite suspension information about the protons involved in the sorption reactions could be extracted. It is important to emphasise that the potentiometric titrations alone cannot be used to measure the sorption. However, combined with sorption data the results from the titrations give priceless input when a surface complexation model for the sorption shall be constructed.

Chapter 3

The oxide/water interface

In equilibrium a charged particle suspended in an electrolyte solution is surrounded by a diffuse cloud of ions. The total charge of this cloud is equal and opposite to the charge of the particle. The arrangement of surface charge and diffuse charge is known as the electrical double layer.

The oxide surface can adsorb and/or desorb protons and that will affect the surface charge on the particles. At low pH the surface charge gets positive and at high pH negative. To distinguish between the charge contributions from electrolyte ions the primary surface charge density σ_o is defined as:

$$\sigma_o = F(\Gamma_{H+} - \Gamma_{OH-}),\tag{3.1}$$

where Γ_i is the amount of adsorbed ions of type i in mol/m^2. The primary surface charge density as a function of pH is the outcome of potentiometric titrations. The point of zero charge pH_{pzc} is defined as the pH-value where σ_o equals zero. This is an important, model independent parameter, which can be determined experimentally.

3.1 Surface groups and mass law equations

A common and accepted symbolism for oxide surfaces is to introduce the concept of surface groups (sites) by a general hydrolysed species, $\equiv$XOH. The loss and gain of protons can then be considered as acid-base reactions at the surface. From a crystallographic point of view the surface hydroxyl groups may be coordinated to one, two, or three underlying metal atoms. It is also possible that two surface groups are attached to one metal atom. See Fig. 3.1 where different types of sites on an iron oxide surface are depicted.
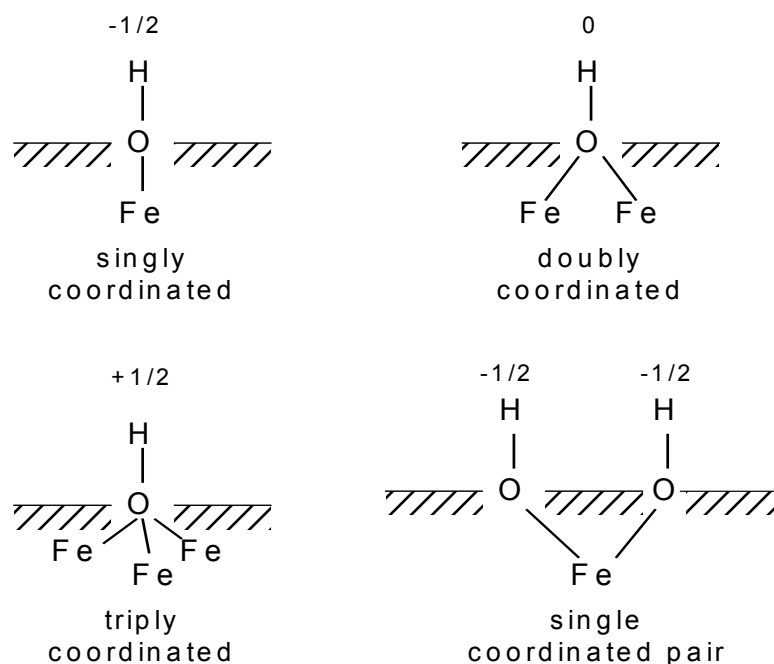
Figure 3.1   Different coordinations of the surface groups on an iron oxide surface. The values represent formal charge numbers of the surface groups. Figure redrawn from Ref. [11].

The configurations of the different types of surface groups depend on the crystal structure of the oxide but also on the crystal face being studied. It is likely that the different surface groups have very different chemical properties. Hiemstra and coworkers have developed a multisite complexation model (MUSIC), where the different surface groups are described in more detail [12, 13]. One of the conclusions from the MUSIC model is that the proton affinity of a surface oxygen atom originates from the undersaturation of the oxygen valence. Their results indicate that it is often only a few different types of surface groups that are active in the titrable pH-range. To be able to apply the MUSIC model to its full extent it is necessary to have detailed information about the relative amounts of different surface planes on the particles. This information is seldom available for mineral particles present outside the laboratory.

The early surface complexation models of metal (hydr)oxides [2, 14] assume that the surface contains one type of reactive surface group that can undergo two protonating steps, i.e.

$$\equiv XOH_2^+ \ \rightleftharpoons \ \equiv XOH + H^+ \tag{3.2}$$

$$\equiv XOH \ \rightleftharpoons \ \equiv XO^- + H^+ \tag{3.3}$$

A mass law equation and an equilibrium constant K_a (proton affinity constant) describe each step. A model based on these two reactions is called a 2-pK model.

Another possibility is to describe the surface reactions with protons in a one step charging process, i.e.

$$\equiv XOH_2^{1/2} \;\rightleftharpoons\; \equiv XOH^{-1/2} + H^+ \tag{3.4}$$

This is called a 1-pK model and was introduced by Bolt and van Riemsdijk [15, 16]. The proton affinity constant in this model follows directly from the experimentally determined pH_{pzc} of the oxide. In Fig. 3.2 the distribution diagrams of the acid/base surface species for the 1-pK and the 2-pK models are compared.
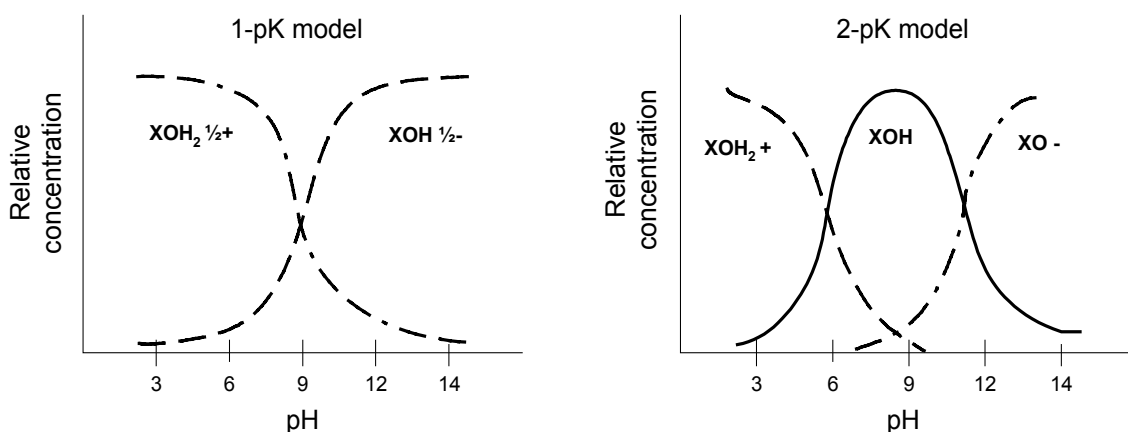

Figure 3.2   Distribution diagrams of the acid/base surface species for the 1-pK and the 2-pK models.

The 1-pK and the 2-pK approximations (models) have been tested and the results reported in an article by Borkovec [17]. He modelled the ionization of the solid/water interface by formulating the problem in terms of a discrete charge Ising model. It was found that for most solid/water interfaces the 1-pK approach represents an excellent approximation to the ionisation behaviour. The reason for this success is the validity of the mean field approximation, which is justified due to the long-range character of the site-site interaction potential.

3.2 The liquid part of the electrical double layer

For a complete surface complexation model a description of the liquid just outside the charged surface has to be added to the proton-binding model. This is of utmost importance since the reacting species are electrostatically affected by the surface charge and the electrostatic potential profile. The most commonly used models are the diffuse layer model (DLM), the basic Stern model (BSM), the constant capacitance model (CCM), and the triple layer model (TLM). For a review see e.g. Ref. [18]. There also exist models called three- and four plane models [19, 20]. These are normally combined with the MUSIC concept for description of the different surface groups. In all electrostatic models mentioned above, except the CCM, a diffuse layer is included. Among them the DLM is the

simplest one, containing only the charged surface and a diffuse layer. Below we shall start to describe the diffuse layer and then the BSM, which has been used extensively in this work.

3.2.1 Gouy-Chapmann theory and the electrostatic correction factor

The diffuse layer in the models mentioned above is based on the Gouy-Chapman theory [21, 22] where the following assumptions have been made:

- The ions in the solution are assumed to be point charges.
- Correlations between the ions in the solution are not taken into account.
- The surface charge is homogeneous.
- The liquid is homogeneous and the dielectric constant ε is not affected by the electric field from the surface.
- The concentration of protons at some location, i, in the electrical double layer is related to the bulk concentration $[H^+]$ by the Boltzmann distribution, e.g.,

$$[H^+]_i = [H^+] \exp\left(-\frac{e\psi_i}{k_B T}\right), \tag{3.5}$$

where Ψ_i is the electrical potential, e the elementary charge, k_B the Boltzmann constant and T the absolute temperature.

In surface complexation models developed so far the analytical solution of a flat and uniformly charged surface is used for the relation between the charge density and the electric potential at the surface. The so obtained surface potential Ψ_0 is then used in an electrostatic correction factor in the expression for the equilibrium constant as described below.

The mass law equation for the 1-pK model coupled to Eq. 3.4 is

$$K_a = \frac{\{\equiv XOH^{-1/2}\}\{H^+\}}{\{\equiv XOH_2^{1/2}\}} \tag{3.6}$$

Because of electrostatic effects the concentration of protons near the charged surface will be different from the concentration in the bulk and since the surface charge is controlled by the pH the equilibrium constant K_a defined as above will change with pH. In surface complexation theory this is overcome by the definition of intrinsic equilibrium constants K_a^{int} for the surface reactions. The apparent equilibrium constant in Eq. 3.6 is then corrected for the electrostatic energy by using the Boltzmann distribution law (Eq. 3.5) and we get

$$K_a = K_a^{int} \exp\left(\frac{e\psi_0}{k_B T}\right) \tag{3.7}$$

K_a^{int} is therefore an equilibrium constant that has been decoupled from electrostatic effects and does not vary with surface charge. At its first sight this way to separate the electrostatic part of the nonideal effects from other contributions to nonideality may seem awkward. In fact, the surface complexation model based on this approach contains inherently some extra-thermodynamic assumptions. For example, the ratio of the surface activity coefficients is taken to be unity. However, the approach has proven to be thermodynamically sound and coherent. The arguments will not be repeated here; instead the interested reader is referred to Refs. [4, 23].

3.2.2 The basic Stern model and Parzons-Zobel plots

If the finite size of the first layer of ions closest to the surface is considered the diffuse double layer model extends to the basic Stern model (BSM) [24]. It means that a charge free layer with a linearly falling electrostatic potential between the charged surface and the diffuse layer is introduced. The model is also often referred to as the Gouy-Chapmann-Stern-Graham (GCSG) model [25]. The capacitance of the Stern layer is defined as:

$$C_s = \frac{\varepsilon \varepsilon_0}{\delta} ,$$

(3.8)

where δ is the distance from the surface to the Stern plane. The capacitance shall be considered as an empirical fitting parameter of the model. Often in the interpretation of C_s the thickness of the Stern layer δ is not only representing the ion size, but also a hydration layer of water molecules where the screening ions cannot enter.

The Stern layer and the diffuse layer can be interpreted as two capacitors in series. The overall capacitance C_{tot} of the double layer then becomes:

$$\frac{1}{C_{tot}} = \frac{1}{C_s} + \frac{1}{C_d} ,$$

(3.9)

where C_d is the diffuse layer capacitance. This division of the liquid part of the electrical double layer is identical to the one performed by Parsons and Zobel when they developed a test for specific adsorption of ions on a Hg electrode [26]. They plotted $1/C_{tot}$ against $1/C_d$ at constant charge and if a straight line of unit slope was obtained they concluded that specific adsorption was absent. If the capacitances C_{tot} and C_s are written in the unit F/g instead of F/m^2 we get

$$\frac{1}{C_{tot}} = \frac{1}{C_s} + \frac{1}{S_{EC}C_d} ,$$

(3.10)

where S_{EC} the electrochemical surface area (m²/g). In this form the equation can be used for the analysis of surface charge data of suspended colloidal particles. This was first done by Siviglia *et al.* on RuO_2. [27]. C_d is dependent on the ionic strength and can easily be calculated. C_{tot} can be obtained from the slope of the experimental surface charge curves. A plot of $1/C_{tot}$ versus $1/C_d$ results in a straight line with a slope inversely proportional to S_{EC} and an intercept providing the value for C_s. In Fig. 3.3 the results from such an analysis on surface charge data of goethite in $NaClO_4$ is shown. How the results from the Parsons Zobel (PZ) -plot can be used in the surface complexation modelling procedure will be illustrated in section 3.3.
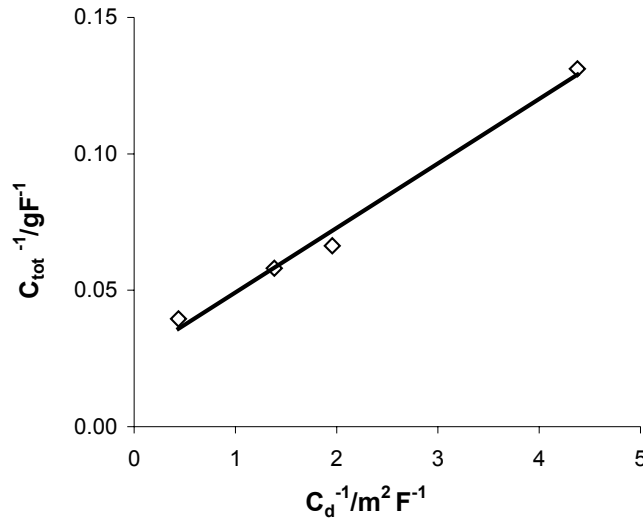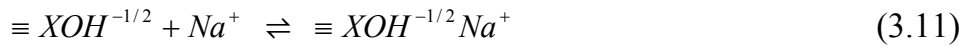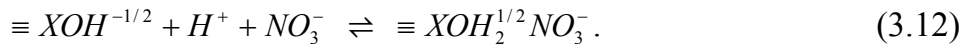

Figure 3.3. Parzons-Zobel plot of titrated surface charge data of goethite in $NaClO_4$. For this data set the electrochemical area (42.4 m²/g) is very close to the measured BET area (40.3 m²/g) of the goethite particles. The value of the inner layer capacitance obtained from the PZ plot is 0.92 F/m². Reprinted from Paper III.

3.2.3 Ion pairing

The Stern layer model can be used with or without adsorption of electrolyte ions in the Stern plane [28, 29]. This is commonly referred to as ion pairing. It can be appropriate for ions that form outer sphere complexes with the surface sites or for ions that are strongly adsorbed to the surface but have no affinity for the proton sites located at the surface plane. If the inert electrolyte is $NaNO_3$ then the adsorption of Na^+ and NO_3^- in the Stern plane can be expressed as:

$$\equiv XOH^{-1/2} + Na^+ \quad \rightleftharpoons \quad \equiv XOH^{-1/2}Na^+ \tag{3.11}$$

and

$$\equiv XOH^{-1/2} + H^+ + NO_3^- \quad \rightleftharpoons \quad \equiv XOH_2^{1/2}NO_3^-. \tag{3.12}$$

When the adsorption of electrolyte ions is taken into account a large fraction of the potential fall will take place in the Stern layer. This is not the case when the BSM model is used without adsorption of electrolyte ions. Model calculated

surface charge curves are also different for the two versions of the BSM. These differences are shown in Fig 2.4 below, where a comparison with a titrated surface charge curve is also made.
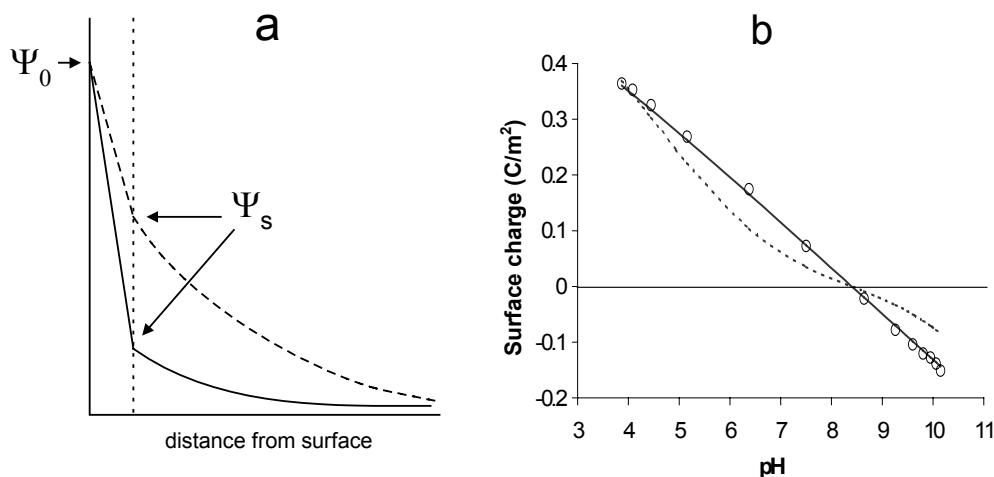

Figure 3.4   Differences between the basic Stern model used with (solid line) and without (dotted line) binding of electrolyte ions in the Stern plane. **a)** Potential fall outside a positively charged surface (pH 4) in 0.1 M NaNO$_3$ and **b)** model calculated surface charge curves. The rings represent experimental data in 0.1 M NaNO$_3$ on colloidal hematite from Paper I.

It is important to emphasise that ion pairing is not always necessary to produce a good fit to experimental surface charge data. Both in Paper III and VI a good description of titrated surface charge on goethite in 0.01 to 1.0 M NaClO$_4$ could be obtained without accounting for ion pairing. In paper III the basic Stern model described above was used and in paper VI a statistical mechanical approach that will be described in chapter 4 was used.

3.3 Titrated surface charge of iron oxide minerals

Potentiometric titrations have been performed on hematite particles of different sizes. When the surface charge curves are calculated particle size is taken into account via the measured BET areas. Yet, significant differences between surface charge curves obtained on the different sets of hematite were found. However, it is a well-known feature that surface properties of colloidal particles often are sensitive to the mode of preparation and history of the sample. When repeated titrations were performed on particles from the same suspension the reproducibility was normally good (differences within 2 %). Within each study we have therefore used particles from the same suspension. In Fig. 3.5 titrated surface charge curves obtained from particles used in Paper I and II are compared. In Paper I we used the larger particles of diameter ~ 0.6 μm (BET area 6.36 m^2/g) and in Paper II particles of diameter ~ 0.1 μm (BET area 16.7 m^2/g) were used. For both of these sets of particles the BET area is higher than the area calculated based on particle geometry obtained from the SEM images. This is

probably due to surface roughness and perhaps to some extent to a fraction of smaller particles.
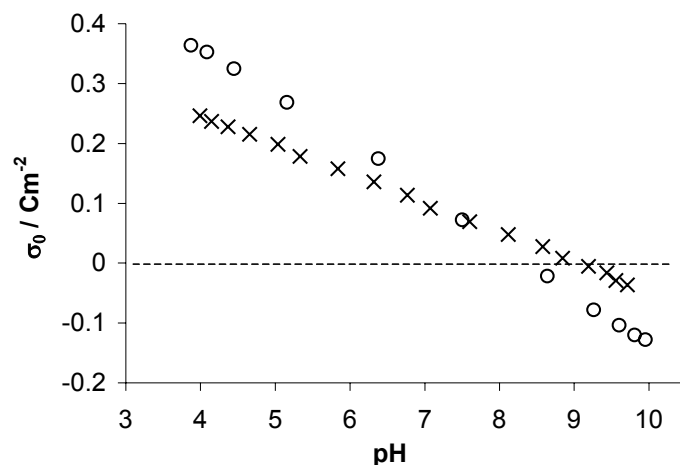

Figure 3.5 Titrated surface charge in 0.1 M NaNO$_3$ for two different sets of hematite particles; ($\times$) particles of diameter ~0.1 μm and BET area 16.7 m^2/g; ($\circ$) particles of diameter ~0.6 μm and BET area 6.36 m^2/g.

It is seen in Fig. 3.5 that the surface charge is higher for the larger particles of lower BET area. Similar differences between titrated surface charges on different goethite (α-FeOOH) samples have been observed independently by Hiemstra & van Riemsdijk [30] and Boily *et al.* [19]. They both measured a higher surface charge density on particles of lower BET area. Furthermore, there is a difference between the pH_{pzc} for the two different sets of particles used in this work.

Much effort has been devoted to find out if the hematite and the goethite surfaces become saturated with protons at lower pH values. If this is the case, it can be a way to experimentally determine the site density, which is an important parameter in the model calculations. Titrations down to pH values lower than three were therefore performed but no clear saturation of protons could be established. The pH measurements at these low pH values are made difficult by experimental problems arising from high liquid junction potentials and possible dissolution of the solid material. Recently, Lützenkirchen *et al.* [31] studied these matters in detail and found that no saturation occurred on goethite down to pH = 2.2 and most probably not even until pH = 0.9 in 0.6 M NaCl. From these results we concluded that it is better to use a surface site density estimated from surface hydroxyl configuration data.

To find a simple and reasonable surface complexation model we started to compare a few different models and their ability to describe titrated surface charge data. First, the possibilities of finding a unique solution of fitted parameters for the 1-pK and the 2-pK CCM to one hematite titration performed in 0.1 M NaNO$_3$ were compared. The experimental curve was aligned in a

straight line (see Fig. 3.5) and both models were able to describe this satisfactory. However, for the 2-pK model it was difficult to determine accurate unique values of the fitted capacitance and the difference between the two equilibrium constants ΔpK_a. We therefore concluded that, based on the success of finding unique parameters, a 1-pK model has major advantages compared to a 2-pK model (Paper I). In chapter 4 where the theoretical foundations of surface complexation are reformulated using statistical mechanics we will also use a charging mechanism corresponding to the 1-pK approximation.

The constant capacitance model is not useful for modelling data at different ionic strengths. In additions, there is no sound way to incorporate measured ζ-potentials into that simple model description. If instead the 1-pK basic Stern model (BSM) is used both these things can be treated realistically. This model has been suggested as a first choice model by some authors [29, 32] and it was the model we decided to use. To get reasonable agreement between experimental titration data and model calculations it was necessary to account for adsorption of electrolyte ions in the Stern plane. In figure 3.6 experimental titration data from Paper II on small (~0.1 µm) hematite particles in 0.01 M, 0.1 M and 1.0 M NaNO$_3$ is shown together with the model curves obtained with the 1-pK BSM. The complete set of model parameters is tabulated in Table 3.1.
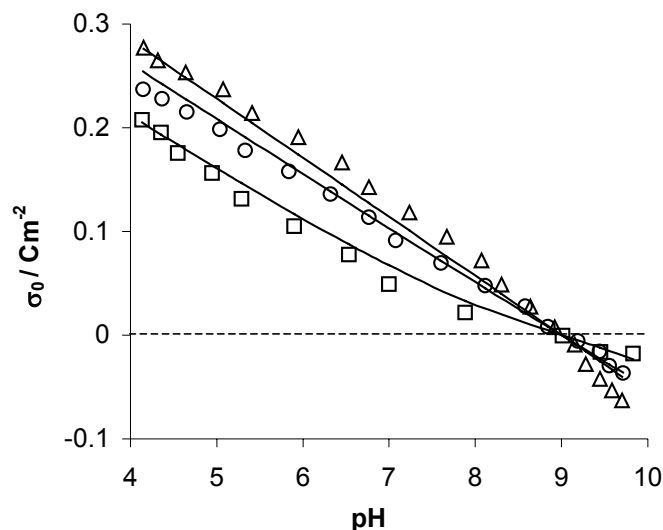

Figure 3.6   Surface charge curves obtained from potentiometric titrations of hematite particles (~0.1 µm) in 0.01 M (□), 0.1 M (○), and 1.0 M NaNO$_3$ (Δ). The solid lines represent model calculated surface charge curves using the 1-pK basic Stern model. Reprinted from Paper II.

Table 3.1 Model parameters for the 1-pK basic Stern model fitted to titrated surface charge of hematite in $NaNO_3$. The site density refers to the total concentration of $\equiv FeOH^{-1/2}$-groups on the surface.

Parameter	Comment
H^+ eq. at the surface plane	*Eq. 3.4*
Site density = 10 nm^{-2}	Fixed value.
LogK$_a$ = -9.0	Fixed value taken from measured IEP.
Electrolyte eq. at the Stern plane	*Eq. 3.11 and 3.12*
logK$_{Na+}$ = 0	Symmetrical fitted constants,
logK$_{NO3-}$ = 9.0	i.e. one adjustable parameter.
Capacitance = 1.03 F/m^2	Fitted parameter

The ionic strength dependence of the surface charge can be understood from the fact that when the electrolyte concentration increases the potential falls off more rapidly outside the surface. In other words, the surface charge becomes better screened by the salt ions. The work of bringing other ions, in this case protons, close to the charged surface is therefore decreased, leading to a higher surface charge at higher electrolyte concentrations.

To minimize the number of adjustable parameters in the modelling procedure attempts have been made to use the Stern layer capacitance of the electrical double layer obtained from Parsons-Zobel (PZ) plots described in section 3.2.2. In Paper III the approach was tested on hematite and goethite data from our own laboratory. In addition, data for Fe_3O_4, TiO_2, and RuO_2 were extracted from the literature and analysed and modelled in the same way. The approach was very successful when applied to the titrated surface charge data of goethite in $NaClO_4$. The electrochemical area and the BET area were very close and the results from 1-pK BSM calculations fitted the experimental data almost perfectly, Fig. 3.7.
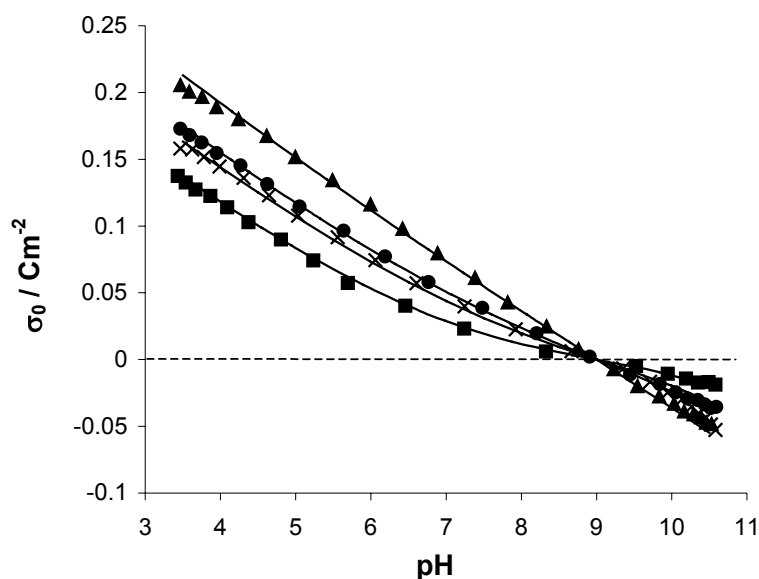
Figure 3.7   Fit of titrated surface charge of goethite in 0.01 (■), 0.05 (×), 0.1(●), and 1.0 M (▲) NaClO$_4$ to the 1-pK basic Stern model. The Stern layer capacitance (0.92 F/m^2) was taken from the PZ-plot and the site density (6 per nm^2) was estimated from crystallographic considerations. No ion pairing of electrolyte ions into the Stern plane was necessary. Reprinted from Paper III.

The agreement for some other oxides was far from perfect. The electrochemical area was substantially higher than the BET area and the model could only give a poor description of experimental surface charge data. Some of these discrepancies may be related to the assumed particle geometry in the calculation of the diffuse layer capacitance C_d. This is discussed in more detail in Paper III.

This section will be ended with some comments on differences between the results presented in Fig. 3.6 and 3.7. The data was collected at the same experimental set up and there was no big difference in the stability of the measured potentials. However, in the hematite titrations (Fig 3.6) the background electrolyte was NaNO$_3$ whereas NaClO$_4$ was used in the goethite titrations (Fig 3.7). The NO$_3^-$ ions are known to have higher tendency to form ion pairs than ClO$_4^-$ has [33]. Since the anions are responsible for the main part of the screening in the titration data (pH_{pzc} is high for hematite and goethite) this difference will influence the titrated surface charge.

The main difference in the two data sets is observed at 1.0 M where the trace of the hematite surface charge data is slightly curved. However, this could not be described successfully in the model although strong formation of ion pairs in the Stern plane was accounted for. Instead, it is probable that the main contribution to the difference stems from the different properties of the colloidal particles. The goethite particles look like long needles and the hematite particles can in principle be approximated as solid spheres (Fig. 2.1). In Paper II where the titration data in Fig. 3.6 were analysed together with ζ-potentials measured by the

electroacoustic technique it was found that the effect of coagulation of hematite particles close to the *pH_pzc* was significant. Since the coagulation increases with ionic strength this may be the reason for the behaviour of the hematite 1.0 M data. A similar curvature in titrated surface charge on colloidal hematite has been reported by Schudel *et al.* [34] but not commented further.

3.4 Electrokinetic studies

Very often the standard electrokinetic model is used for describing transport properties of colloidal particles and ions in solution. To describe the system, we start to think of a set of spherical particles of equal size with smooth and homogeneous surfaces. When a particle moves in an arbitrary electrolyte solution a thin liquid layer will move with the particle. The layer between the moving and stationary liquid defines the slip plane and the potential in that plane is the electrokinetic potential also called the ζ-potential. Inside the slip plane the particles are considered to be solid spheres with no bulk conductivity. The interaction between the charged particles and the electrolyte ions in the liquid is described by the Gouy-Chapman theory outlined in section 3.2.1. For a rigorous treatment of the electrokinetic properties of a colloidal system it is necessary to set up a number of coupled partial differential equations, normally referred to as the electrokinetic equations, see e.g. Refs. [35, 36].

When a particular electrokinetic problem has to be solved it is often possible to introduce further assumptions that will simplify the system of equations that have to be solved. By defining appropriate boundary conditions it is then possible to obtain approximate analytical or numerical solutions to the equations. This has led to different simpler expressions for relating measured mobility to ζ-potential.

3.4.1 The ζ- potential

The ζ-potential cannot be measured directly. It has to be calculated from the mobility of the particles. Let us first look at the case when the particles are immersed in a liquid under the influence of a d.c. electric field, i.e. electrophoresis. The electrophoretic mobility μ is then simply defined as the ratio between the speed of the particles and the applied field strength.

If the thickness of the electrical double layer ($1/\kappa$) is much smaller than the radius *a* of the particle, i.e. if $\kappa a \gg 1$, the Smoluchowski's relation between the electrophoretic mobility μ and the ζ-potential is valid [37]

$$\mu = \frac{\varepsilon \varepsilon_0 \zeta}{\eta},$$
(3.13)

where η is the viscosity of the liquid.

Many other expressions relating the mobility to the ζ-potential can be found in the literature but they all have restrictions on the values of κa and/or the ζ-potentials. For good reviews see e.g. Refs. [35, 36]. However, there exist numerical solutions to the electrophoretic problem that is valid for all κa-values and ζ-potentials. One of them has been developed by O'Brien and White [38] and a computer program, Mobility©, exists where the algorithm has been implemented.

In Fig. 3.8 the electrophoretic mobility is shown as a function of ζ-potential using Smoluchowski's equation (Eq. 3.13) and the O'Brien and White theory [38]. In the calculations spherical particles, of radius 60 nm, suspended in 10 mM NaNO$_3$ are assumed. This corresponds to a κa-value of 20. It can be seen that Smoluchowski's equation only gives appropriate zeta potentials for quite low mobilities. The maximum in the mobility arises from the fact that the electrophoretic retarding forces increase faster with ζ than does the driving force [38].
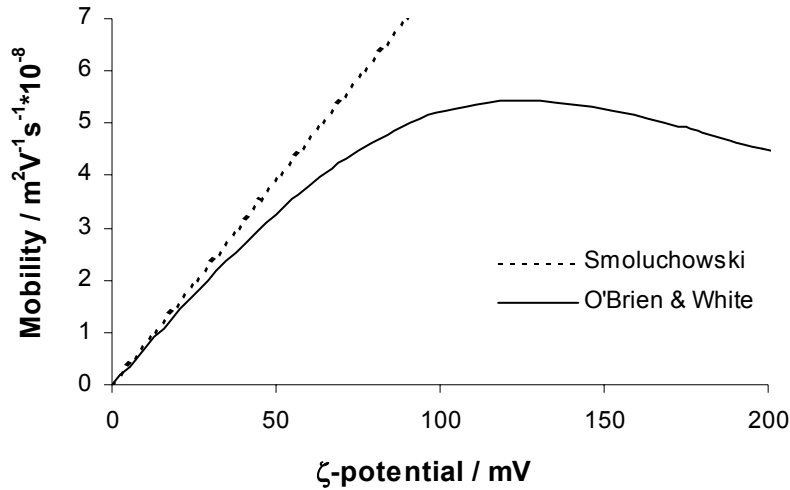

Figure 3.8   Calculated electrophoretic mobility as a function of ζ-potential using Smoluchowski's equation and the theory of O'Brien and White [38]. Spherical particles, of radius 60 nm, suspended in 10 mM NaNO$_3$ are assumed ($\kappa a = 20$).

Let us now go to the dynamic case when the particles move under the influence of an a.c. field. If the applied alternating electric field is sinusoidal it can be represented by the real part of $\mathbf{E_0}e^{i\omega t}$ and the resulting particle velocity by the real part of $\mathbf{V_0}e^{i\omega t}$. $\mathbf{E_0}$ and $\mathbf{V_0}$ are then complex vectors. These two quantities define the dynamic mobility μ_d according to:

$$\mathbf{V_0} = \mu_d \mathbf{E_0} \tag{3.14}$$

From this definition it follows that μ_d is a complex quantity of magnitude V/E and argument $\omega \Delta t$ radians [9]. The argument is a measure of the phase difference

19

between the applied field and the particle motion. When the time delay between the applied field and the particle motion is zero, μ_d becomes a real quantity. The dynamic mobility is then the same as the electrophoretic mobility defined for a static applied field.

In the AcoustoSizer software the theory developed by O´Brien is used to calculate the ζ-potentials [8]. The theory uses a thin double layer approximation, and therefore, κa-values less than 20 are not recommended by the manufacturer [39]. A numerical solution of the electrokinetic equations applied to the dynamic case has been developed by Mangelsdorf and White [40]. The solution is applicable to all κa-values. In Paper II this numerical solution as well as the thin double layer approximation were used to fit experimental data on colloidal hematite measured with the AcoustoSizer.

An example of measured magnitudes and phase angles of the dynamic mobility are shown in Fig. 3.9. In this study the small particles shown in Fig. 2.1.a) were used.
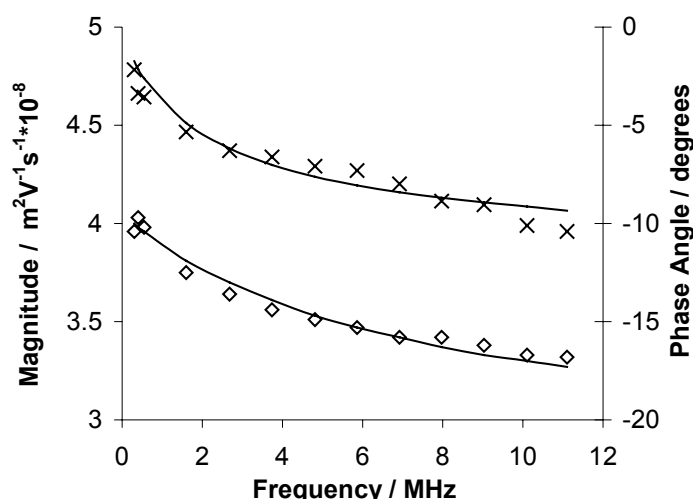

Figure 3.9   Measured magnitudes ($\diamond$) and phase angles ($\times$) of the dynamic mobility of colloidal hematite at pH 4 in 5 mM NaNO$_3$. The lines represent the fit, obtained by the AcoustoSizer software, to O´Briens theory for thin double layers. The ζ-potential in this case was 65.7 mV and the fitted median diameter of the particles was 0.12 μm. Reprinted from Paper II.

It is clearly shown how the phase angles decrease (the phase lag increases) with increased frequencies, i.e. the particles have more difficult to follow the applied field at the higher frequencies. For the same reason the magnitude is decreasing with increasing frequencies.

To produce the fit to the data three fitting parameters have been adjusted: the ζ-potential, the average particle size and the width of the particle size distribution (log-normal distribution assumed). The fitted median diameters ($\sim$0.12 μm from

O´Briens theory and 0.080 μm from the Mangelsorf-White theory) were in reasonable agreement with particle sizes observed in the SEM image. A general feature of the results was that the more accurate theory of Mangelsdorf and White gave slightly higher ζ-potentials than O´Briens theory. This is exemplified by the values obtained from the data in Fig. 3.9: 68.0 mV from the theory of Mangelsdorf and White and 65.7 mV from O´Briens theory.

For the two lowest ionic strengths, 5 mM and 10 mM, good fits to O'Briens theory were obtained by the AcoustoSizer software at pH values lower than 7. Equally good fits to these data were also obtained using the Mangelsdorf-White theory and a log-normal size distribution.

However, at higher pH values and at high electrolyte concentrations (50 mM and 100 mM) the fitting procedure for both theories (O'Brien and Mangelsdorf-White) did not converge or produced a poor fit. This is probably due to pronounced coagulation of the hematite particles. Thus, another method to calculate the ζ-potentials was needed. Fortunately, the measured phase angles were small at the lowest frequency (0.3 MHz) and it was possible to make the approximation that the dynamic mobility is equal to the static electrophoretic mobility and use that value for ζ-potential calculations. In Fig. 3.10 the ζ-potentials obtained from numerical calculations performed according to the theory of O'Brien and White [38] are shown.
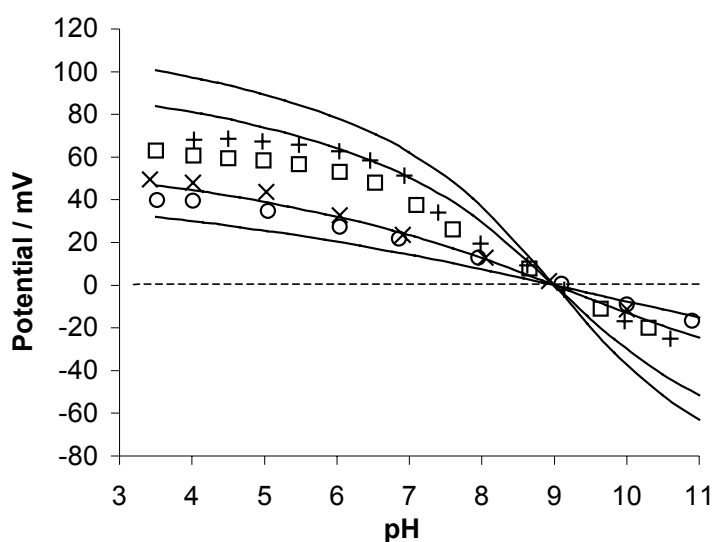

Figure 3.10   Zeta potentials calculated from the experimental mobility data according to the theory by O'Brien and White in 5 mM (+), 10 mM (□), 50 mM (×), and 100 mM NaNO$_3$ (○) as a function of pH. The solid lines represent model-calculated potentials in the Stern plane at the same four ionic strengths. Reprinted from Paper II.

It has already been mentioned that aggregation was a major problem at the higher ionic strengths. To interpret the dynamic mobility data we therefore used a theory for porous particles (flocs of small primary particles) developed by O'Brien [41]. We obtained good fits to the theory for some data points in 100 mM NaNO$_3$ and the so obtained ζ-potentials were in good agreement with the values obtained from the numerical calculations shown in Fig. 3.10. This was a satisfactory result since it justifies the use of the ζ-potentials obtained from O'Brien and Whites theory although the particles form large aggregates.

One of the objectives of the electrokinetic study was to explore if the ζ-potentials could justify the 1-pK BSM obtained from potentiometric titrations on hematite (Fig. 3.6 and Table 3.1). Our suggestion is that the slip plane where the ζ-potentials are measured coincide with the Stern plane in the basic Stern model. Together with the ζ-potentials in Fig. 3.10 we have therefore plotted 1-pK BSM calculated potentials in the Stern plane. It can be seen that qualitatively the model predicts the correct ionic strength dependence of the ζ-potentials. In addition, there is a rather good quantitative agreement for the two highest ionic strengths. However, at 5 mM and 10 mM ionic strength the model predicts up to 40% higher values than found from the electrokinetic study.

3.4.2 Surface conduction

One possible mechanism that is not taken into account in the standard electrokinetic theory is surface conduction behind the slip plane. Accounting for this mechanism means that the assumption that the liquid behind the slip plane is considered to be completely stagnant, moving with the particle, is not valid anymore. Instead the counter ions close to the charged surface will move in a direction tangential to the surface. In studies where the ζ-potential has been determined from both electrophoresis and dielectric response measurements, surface conduction has been introduced to get consistent data from the two techniques [42, 43]. Mangelsdorf and White have extended both the numerical solution for static electrophoresis developed by O'Brien and White but also the full dynamic electrokinetic theory to the situation when surface conduction behind the slip plane is present [44-46].

To analyse how this mechanism would affect the ζ- potentials obtained from our mobility data, numerical calculations using the full dynamic electrokinetic theory were performed. The amount of surface conduction is modelled with a few different model parameters (for details see Paper II). In Fig. 3.11 the magnitudes of the dynamic mobility at 0.3 MHz are shown as dotted lines for the two ionic strengths 10 and 100 mM. In these calculations monodisperse particles of radius 60 nm were assumed.
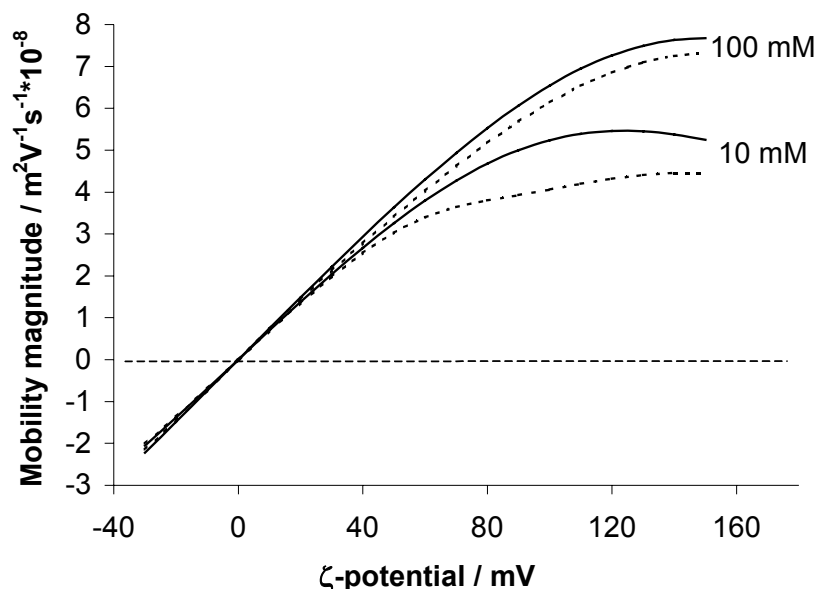
Figure 3.11   Calculated magnitude of the dynamic mobility at 0.3 MHz as a function of ζ-potential for a spherical particle of radius 60 nm suspended in 10 mM and 100 mM $NaNO_3$. The dotted and solid lines represents data calculated with and without surface conduction behind the slip plane, respectively. Reprinted from Paper II.

It can be seen that the effect of introducing surface conduction behind the slip plane is greater for low ionic strengths and high ζ- potentials. It means that the ζ-potentials at the two lowest ionic strengths in Fig. 3.10 will be shifted closer to the model curves in the acidic region. However, the introduction of this mechanism could not completely describe the discrepancies between the ζ-potentials obtained and the Stern plane potentials calculated with the model. Instead, the introduction of the surface conduction shall be seen as a possible mechanism responsible for discrepancies in the ζ-potentials obtained. Another factor is the location of the shear plane. In our 1-pK basic Stern model we have made the assumption that it is located in the Stern plane. Another possibility is to assume the slip plane to be further out in the solution outside the Stern plane [43, 47].

Chapter 4

Statistical mechanical approach to surface complexation

Hopefully it has been demonstrated in the previous section that the concept of surface complexation is very useful for the interpretation and understanding of various features of the oxide/liquid interface. It gives a wide range of chemists a practical tool for creating simple models and the opportunity to put the surface reactions into its proper context with other ongoing phenomena, such as the transportation and sedimentation of suspended particles or the formation of complexes in solution. In that sense the close connection to mass law equations and equilibrium constants used traditionally in solution chemistry is one of the strengths of the surface complexation concept. In chapters 5 and 6 of this thesis where surface complexation models are applied to more complex systems this will be exemplified even further.

However, it cannot be overlooked that there are some problems with the models as they are used today. As the complexity of the models increases it becomes more difficult to unravel the physical meaning behind the fitting parameters involved. The influence from electrostatic effects on reactions at a charged surface cannot be overrated. A natural question is therefore if the assumptions made in the Gouy-Chapmann theory and its variants are reasonable and to what extent are phenomena not accounted for hidden in the equilibrium constants and other model parameters? These questions motivated us to reformulate a theory of surface complexation in terms of statistical mechanics. It is the natural theoretical tool for providing a link between a molecular description and macroscopic measurable properties. The work shall also be seen in the light of the great progress made recently in describing structural aspects of various surface complexes. Experimental techniques such as infrared spectroscopy and EXAFS (extended X-ray absorption fine structure) have become important for molecular input to the models and to work in a context that can fully utilise this information must be a great advantage.

The theoretical development used in the reformulation of a surface complexation theory is based on the generalized van der Waals (GvdW) theory of fluids [48]. In the GvdW approach some basic ideas of cell theory and a density functional approach are used to derive an equation of state for a fluid as well as nonuniform fluid properties such as adsorption excess, surface tension, and screening. In section 4.1 some basic features of the GvdW theory will be discussed but for a

more rigid background and overview the readers are referred to the recent review by Nordholm & Penfold [49]. One of the main advantages of the surface complexation model developed here is that it accounts for the finite size of the ions in the screening atmosphere. In addition, we are not restricted to the planar surface limit; instead the more general case of a spherical particle of arbitrary size is treated. The model also gives a molecular description of the site binding of protons at the oxide surface – the process that regulate the surface charge of the suspended particles.

4.1 Generalized van der Waals theory

As the name indicates the generalized van der Waals (GvdW) theory is a generalization of the theory developed by van der Waals for inhomogeneous fluids. Let us therefore begin by looking at the well-known equation that he proposed for the pressure P of a fluid in terms of the temperature T and volume per particle v

$$P = \frac{k_B T}{v - v_0} - \frac{a}{v^2} \,. \tag{4.1}$$

This kind of relation describing the pressure as a function of temperature and density is called an equation of state. In Eq. 4.1 the interactions between the particles in a fluid enter through two parameters, i.e. v_0, the excluded volume per particle and a, the binding energy per particle at unity density. Note that if the interaction between the particles are neglected the van der Waals equation of state reduces to the ideal gas law, i.e.

$$P = \frac{k_B T}{v} = \frac{N k_B T}{V} \,, \tag{4.2}$$

where N is the total number of particles and V the total volume of the system.

Let us return to Eq. 4.1 and look at the interaction parameters. v_0, the excluded volume per particle, arises due to the short range repulsion of particles of a finite volume. It leads to an entropic effect since it reduces the volume accessible to the particles in the system. The attractive interactions, described by the parameter a, contributes to the energy of the system but are assumed not to affect the motion of the particle and is therefore separable from the entropy. This is called a mean field approximation.

In the GvdW theory the mean field approximation is retained but the derivation is improved and generalized by the use of a cell theory approach. The volume of the system is divided into cells in a cubic lattice. Each cell contains one particle and has a volume $v = N/V$. The restriction that each particle now only has the volume v to move in decreases the entropy of the system. This cell model is a first minor generalization of the van der Waals original derivation. The second generalization is the reinterpretation of the excluded volume per particle v_0. Van

der Waals suggested the value $2\pi d^3/3$, where d is the diameter of the particles which were modelled as hard spheres with attractive tails. A natural excluded volume per particle in the cell theory is $v_0 = d^3$. In the cubic lattice this corresponds to the close packing limit where the side length of the cell wall becomes equal to the diameter of the ion. $v_0 = d^3$ is a lower value than $2\pi d^3/3$ and gives a more realistic behaviour of the fluid in the high-density limit. However, $v_0 = 2\pi d^3/3$ gives a better description in the low-density limit. Therefore a theory called Interpolated GvdW(I) has been developed and it gives accurate results in both limits. The GvdW has been extended to describe many different kinds of systems [49]. The general route is to derive free energy density functionals and from them calculate various properties of the system. For example the GvdW theory can be applied to screening problems in the theory of electrolytes. One example of that is the corrected Debye-Hückel (CDH) theory upon which our analysis of surface complexation is based. The CDH theory will be described shortly in the following section. For a complete derivation see Ref. [50] and Paper IV.

4.2 Corrected Debye–Hückel theory

The corrected Debye-Hückel (CDH) theory is a theory of electrolyte solutions and screening of charged particles and it is based on the GwdW theory described above. In these systems the screening is dominated by long-range Coulombic interactions. In 1984 Nordholm worked out the CDH theory for symmetrical electrolyte solutions [50]. In Paper IV it is extended to describe the screening of not only salt ions but also charged particles of any size. In addition, the derivation is generalized to account also for unsymmetrical salts.

In the CDH theory a linear electrostatic response is assumed but compared with the traditional Debye-Hückel (DH) theory [51, 52] two new mechanisms are introduced namely the excluded volume effect and the hole correction of electrostatic interactions. Ion size effects are accounted for within a restricted primitive model of the electrolyte. It means that the ions are immersed in a solvent of dielectric constant ε and that they are represented by hard spheres of one and the same diameter d. A pairwise additive interaction potential is assumed and it consist of a hard repulsive part and a soft Coulumbic part. The hard part of the potential is a step function, which becomes infinite when the hard spheres overlap and is zero otherwise.

Remarkably the excluded volume effect does not in the linear local entropy approximation contribute to the free energy associated with the screening mechanism. This is due to the perfect cancellation between adsorption of counterions and desorption of coions at every distance r from the particle. This leaves the total ion density the same as in the bulk limit and the screening is then only expressed in the form of a concentration fluctuation at constant total ion density. Note that this cancellation of excluded volume effects on the screening free energy would not apply if the ions were of different size.

For a particle of diameter D and charge number Z in a binary salt solution with ions of charge numbers z_1 and z_2 the total change in Helmoltz free energy of screening is shown to be (Paper IV)

$$\Delta F_{sc} = \frac{k_B T}{n_B} \frac{Z^2}{z_1(-z_2)} \frac{\kappa^3}{16\pi(1+\kappa\hat{D})^2} - \frac{Z^2 e^2}{4\pi\varepsilon\varepsilon_0 \hat{D}} \left[\frac{\kappa\hat{D}}{4(1+\kappa\hat{D})^2}(2+2\kappa\hat{D}+\kappa d+\exp(-\kappa d) \right],$$

(4.3)

where n_B is the bulk ion density (in ions per m^3) and $\hat{D} = (D+d)/2$. The first term on the right hand side of Eq. 4.3 is the cost in free energy due to loss of entropy as the salt ions are arranged into a screening atmosphere. The second term is the lowering of electrostatic energy achieved by formation of the screening atmosphere. The terms including the diameter d of the salt ions account for the hole-correction of electrostatic ion-ion interactions associated with the ion size. The parameter κ which describes the inverse screening length of the diffuse layer shall be obtained by minimizing the free energy in Eq. 4.3. The electrostatic hole correction weakens the repulsion between the screening ions which results in a higher value of κ than the "Debye-Hückel-κ". It means that the screening is more efficient than in the original DH theory. This is shown in Fig. 4.1 where the dimensionless screening parameter κd is plotted as a function of concentration. In these calculations d was set to 0.425 and 0.42 nm for 1:1 and 2:2 electrolytes, respectively. It can be seen that higher κd-values are always obtained with the CDH theory compared to the original DH theory where the ion size in the screening atmosphere is neglected. The effect is most pronounced for 2:2 electrolytes which may be explained by the fact that 2:2 electrolyte solutions are more strongly coupled that 1:1 electrolytes.
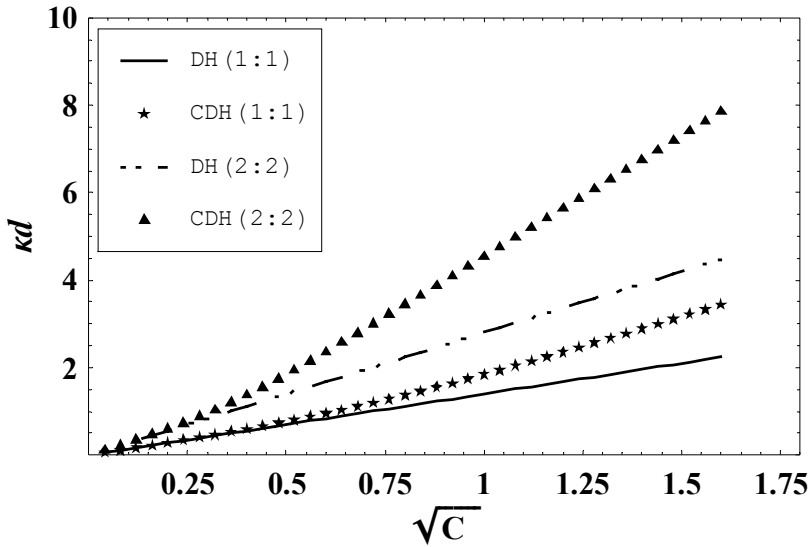

Figure 4.1 The dimensionless screening parameter κd is shown as a function of the square root of the molarity. DH is the Debye-Hückel predictions whereas CDH is the corrected Debye-Hückel predictions obtained here for 1:1 and 2:2 salts (from Paper IV).

In Paper IV the extended derivation of the CDH theory was tested by application to the bulk salt limit. Thermodynamic properties such as the internal energy, osmotic coefficient and mean ionic activity coefficients were calculated and compared with simulation results and experimental data. The agreement between the CDH and the MC simulation results was generally very good over a wide range of concentrations from 0 to 2 M in most cases. Notable deviations were seen mainly for 2:2 electrolytes where the coupling is so strong that the linear response assumption is certain to be significantly violated. In Fig. 4.2 an example is given where the CDH calculation of the mean activity coefficients have been compared with simulation data obtained by Van Megen and Snook [53]. Note that these CDH calculations are a priori, i.e. no fitting parameter has been used to obtain the agreement. The characteristic upward curvature of graphs of ln γ as function of $\sqrt{C}$ is due to the hard sphere effects normally neglected in the Debye-Hückel theory.
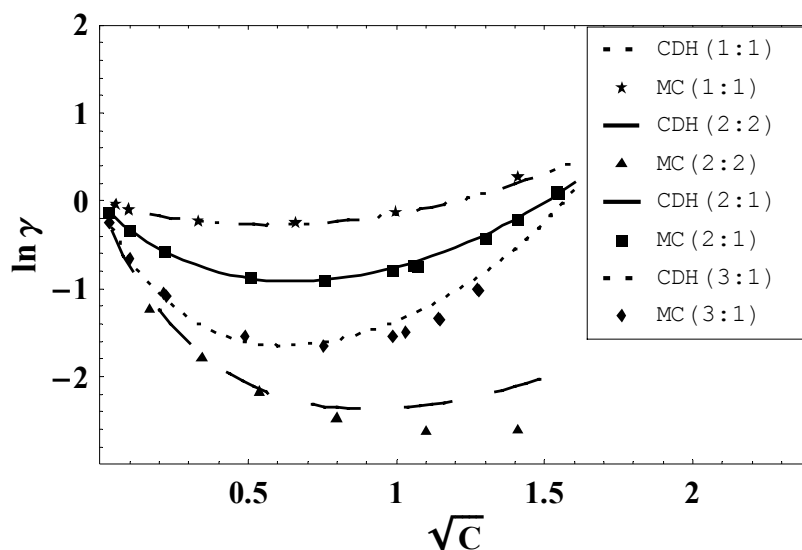

Figure 4.2   The natural logarithm of the mean ionic coefficients is plotted as a function of the square root of the molarity. Results obtained for RPM electrolytes by the CDH theory are compared with Monte Carlo (MC) simulation results from Ref [53]. Reprinted from Paper IV.

In the comparison with experimental data it was first necessary to determine a best fitting diameter *d* for each salt. Fortunately this was possible to do by inspection since the diameter was found to fall in the physically expected range. In general, the resulting fit was satisfactory up to concentrations above 1 M. An example is given in Fig. 4.3 where mean activity coefficient data of Robinson & Stokes for NaCl and KCl [54] have been fitted by the CDH theory.
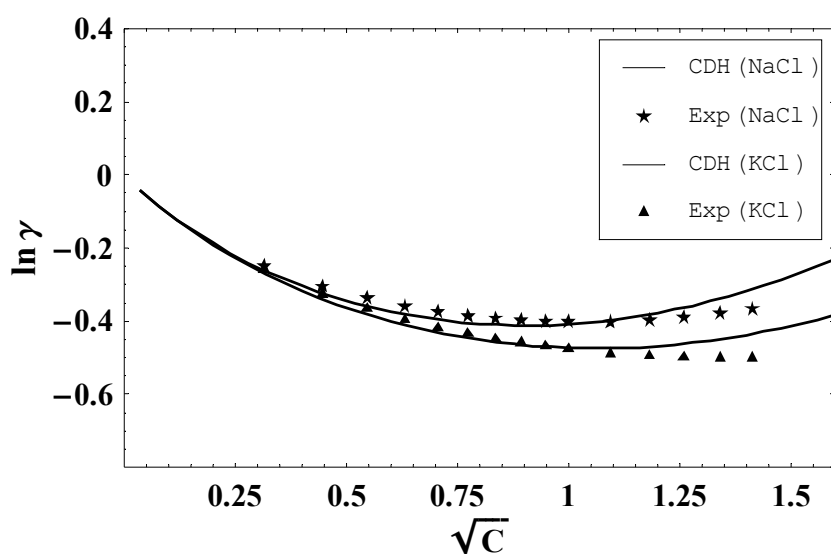
Figure 4.3   The natural logarithm of mean ionic activity coefficient as function of the square root of the molarity for NaCl and KCl. CDH denotes the corrected Debye-Hückel theory and Exp the experimental results from Robinson and Stokes [54]. The best fitting diameters used in the CDH calculations are 0.34 and 0.31 nm for NaCl and KCl, respectively. Reprinted from Paper IV.

The mean diameters from the CDH fit were 0.34 nm for NaCl and 0.31 nm for KCl. These values are closer to the average Pauling type diameters (0.282 nm and 0.318 nm for NaCl and KCl, respectively) than to the average hydrated diameters. Preliminary results from calculations using a refined implementation of the CDH theory for bulk thermodynamic properties where the concentration dependence of the dielectric constant have been included show that the fitted diameters increase slightly and the applicability range can be extended to ~3 M [55]. An extensive study of effective diameters in the CDH theory for salt solutions has been performed but is not included in this thesis [56]. Calculations were performed on 67 different salts and the CDH results were compared with other more empirical models for describing bulk thermodynamic properties.

4.3 The site binding mechanism

The CDH analysis described so far can resolve the screening of a charged surface/particle but not fundamentally predict the charge itself since this invariably requires short range binding mechanisms to be resolved. This was first done in Paper V where the planar limit was explored. A refined model is presented in Paper VI where the more general case of a spherical particle of arbitrary size is treated. However, the models are very similar and the parameters for the site binding are identical. The revised implementation in Paper VI was necessary to be able to describe also the stepwise charging of very small particles with low charge numbers. Furthermore, the latest version of the theory is focused more on the equilibration of chemical potentials rather than the minimization of free energies as done in the first implementation. The two approaches must yield

the same results within the same model and theory but the equilibration of chemical potentials is the traditional method of choice.

As described in detail in section 3.2 the surface reactions in SCMs developed so far are modelled via mass law equations and equilibrium constants. In our CDH analysis we have chosen to proceed quite differently. The binding of protons at the surface sites will be described as an harmonic oscillator, which is modelled in terms of a binding energy u_0 and a three-dimensional vibration of frequency v.

Let us assume that we have a spherical particle and that the total number of bonding sites on the particle is M and that N of these are occupied by protons. The charge (in C) of the particle will then be

$$Ze = (N - N_n)e, \qquad\qquad (4.4)$$

where N_n is the number of occupied sites when the particle is neutral. The proton adsorption-desorption mechanism can take the particle charge number Z between the lower limit $-N_n$ and the upper limit $M-N_n$. A one step charging process will be assumed and N_n will be set equal to $M/2$ in our discussion below. It means that the theoretical development has been based on a site model corresponding to the 1-pK charging mechanism (Eq 3.4).

By using combinatorial arguments and an estimate of the electrostatic energy associated with the stepwise adsorption of protons on to the charged particle the chemical potential of the bound protons μ_b can be derived. The equilibrium condition for the proton exchange is, if no screening of the central particle is accounted for, that the chemical potential of a proton on the surface site is the same as the chemical potential of a free proton in the solution μ_f, i.e.,

$$\mu_f = \mu_b. \qquad\qquad (4.5)$$

μ_f is a function of the pH-value in solution and does not depend on any properties of the particle. By solving Eq. 4.5 the equilibrium value of the number of adsorbed protons, i.e. the particle charge will be obtained. If this is done repeatedly for a range of pH-values one will get a surface (particle) charge curve corresponding to those discussed in chapter 3. Note that in Eq. 4.5 the screening of the charged particle by electrolyte ions has been completely ignored and therefore the magnitude of the charge will be strongly underestimated. However, this simple equation will show a correct pH_{pzc} and can be used to determine the site binding parameters v and u_0 for a specific oxide surface with a well-known pH_{pzc}. This was done for a large particle of a diameter of 100 nm and the results are shown in Fig. 4.4 where couples of the two parameters hv (h is Planck's constant) and u_0 that yield zero surface charge at different pH-values are presented.
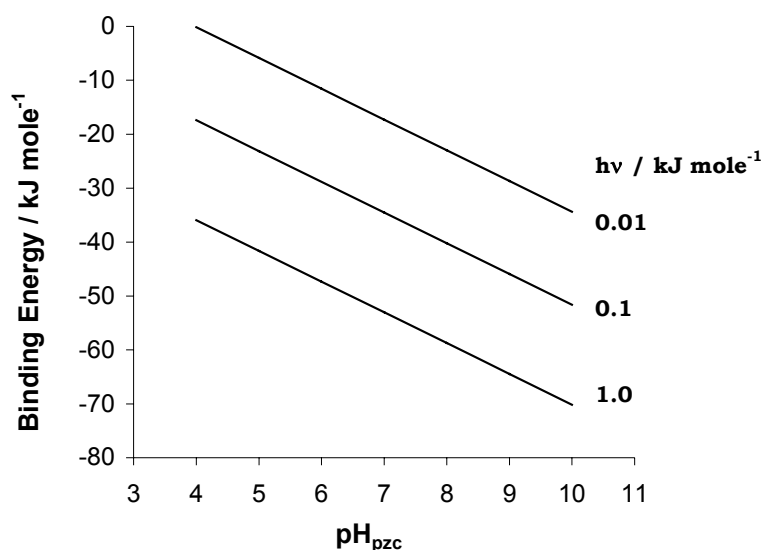
Figure 4.4   The binding energy u_0 shown as function of pH_{pzc} for three different values of the vibration frequency hv.

It is seen that for a specific pH_{pzc} we cannot uniquely determine the two parameters. Assume for example that $pH_{pzc} = 8.0$. This can be modelled with hv = 1.0 kJ/mole and $u_0 = -58.7$ kJ/mole or $hv = 0.01$ kJ/mole and $u_0 = -23.0$ kJ/mole. The number of combinations is infinite. However, the vibration frequency hv will affect the temperature dependence of the pH_{pzc}. This is shown in Fig 4.5 where the model calculated temperature dependence has been fitted to the experimental data of Fokkink *et al.* [57] on hematite. Using this approach hv could be locked to 0.35 kJ/mole.
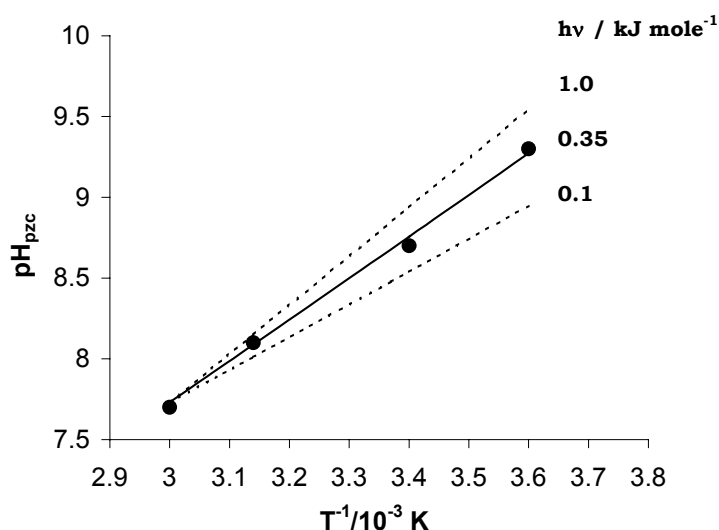

Figure 4.5   The temperature dependence of the pH_{pzc} calculated using three different vibration frequencies hv: 1.0, 0.35 and 0.1 kJ/mole. The corresponding binding energies were -63.3, -53,6 and -42.8 kJ/mole, respectively. The point represents experimental data of Fokkink *et al.* on colloidal hematite [57].

4.4 Screening of a charged particle

4.4.1 Linear screening with capacitor layer included

If we account for the response of the solution to the presence of a charged particle, the salt solution will lower its free energy by letting its counterions to the particle accumulate in a screening atmosphere and the coions in the same way be depleted in this screening atmosphere. If the screening is not too strong, Eq. 4.3 can be used to describe the free energy change associated with the screening. Since the finite size of the ion is accounted for a thin charge free layer of thickness $d/2$ will be present close to the charged surface. This corresponds to a Stern layer in its very simplest form. However, it is generally thought that the ions are separated from the surface not only by their own size but also by a hydrating layer of water molecules at the surface. This layer is impenetrable to the salt ions and within the CDH analysis we call it a capacitor layer. Let us now correlate this model of the region next to the charged surface with the description given in section 3.2.2 where the basic Stern model was discussed. In that model the ions are represented by point charges and the thickness of the Stern layer (δ in Eq. 3.8) accounts for both the ion size and what we here call the capacitor layer. The thickness of the capacitor layer w_c and δ are therefore related to each other as

$$\delta = w_c + d/2.\tag{4.6}$$

In paper V the energy per unit area of the capacitor layer in the planar limit was obtained as

$$f_C(\sigma) = \frac{2\pi\sigma^2 w_c}{4\pi\varepsilon\varepsilon_0},\tag{4.7}$$

where σ is the surface charge density (C/m^2). Notice the appearance of the ratio w_c/ε in this expression and that the iverse ratio is present in Eq. 3.8. To be able to say something about the thickness of the Stern layer/capacitor layer it is necessary to have an idea about the dielectric constant ε close to the charged surface. This is a non-trivial task since ε is a bulk thermodynamic property and from a theoretical point of view it loses its validity on a molecular scale. Nevertheless, the strong electrostatic field close to a charged surface will lead to a lower value of ε in the Stern layer/capacitor layer than in the bulk (~78). In the CDH algebra we have not distinguished ε in the capacitor layer from the bulk value. However, the values of the thickness obtained can always be reinterpreted in terms of a lower dielectric constant. This is discussed in more detail in Paper V.

In the case of a spherical particle (Paper VI) the capacitor layer was introduced in a slightly different way. Since $\hat{D} = (D+d)/2$ is the radius where the screening starts if no capacitor layer is present we can just define a new radius $R_c = \hat{D} + w_c$ and let the screening start there, see Figure 4.6. It means that we can use Eq. 4.3 without any additional free energy for the capacitor layer if we replace $\hat{D}$ by R_c.
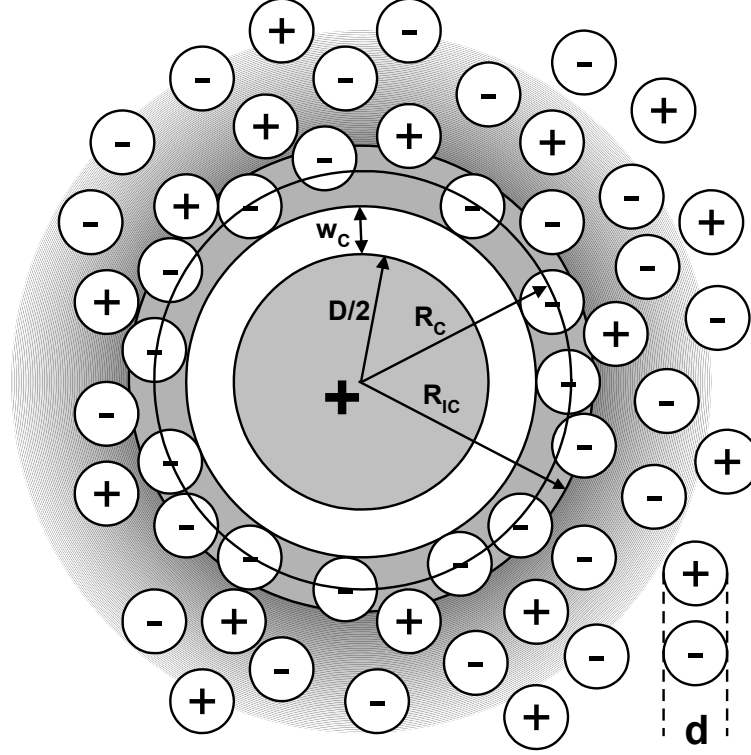

Figure 4.6   Schematic drawing of the proposed model for particle screening. The particle is assumed to be positively charged. The central solid particle has a diameter D and the screening ions a common diameter d. The surface charging mechanism of proton adsorption and desorption takes place at the particle surface ($r = D/2$). The white area next to the particle surface represents the capacitor layer (thickness w_c) where the screening ions cannot enter. The point of closest approach of the centre of the screening ions is at $r = R_c = D/2 + w_c + d/2$. In the interval $R_c < r < R_{ic}$ the condensation of counterions takes place and at $r = R_{ic}$ the field criterion is precisely satisfied. For $r > R_{ic}$ the screening is represented by a linear CDH diffuse layer. Reprinted from Paper VI.

The chemical potential of the linear CDH screening with capacitor layer included μ_{sc} can now be obtained from the derivative of ΔF_{sc} (Eq. 4.3.) with respect to the number of adsorbed protons N which is related to the charge number Z. The equilibrium condition for the proton exchange now becomes

$$\mu_f = \mu_b + \mu_{sc}, \tag{4.8}$$

where we just have added the contribution from the screening mechanism to the chemical potential of a bound proton. This equation can then be solved for Z at a specific pH-value and salt concentration to obtain the particle charge.

In the following, model calculated surface charge curves are compared to the surface charge data of goethite in $NaClO_4$ solution. The different mechanisms are introduced step by step to clearly show the effect on the model calculated surface charge. The diameter of the central particle was set to 100 nm and the diameter of the screening ions to 0.425 nm. With this large central particle results almost equal to those found in the planar limit were obtained. First the binding energy u_0 was adjusted to get a $pH_{pzc} = 9.0$. The site binding parameters u_0 and hv are then kept locked and cannot be used as fitting parameters for the surface charge curves.

In Fig. 4.7 results from calculations performed with a background salt concentration of 0.1 M are shown. From the difference between curve 1 and 2 it is clearly seen how the finite size of the screening ions affect the surface charge. At this level of the theory none of the model parameters have been used as fitting parameters (The site density is fixed to 6 sites per nm^2). In curve 3 a capacitor layer is also included. The capacitor layer weakens the screening mechanism and thus decreases the charge of the particle at any given salt concentration and pH of the solution. The thickness w_c is used as a fitting parameter (0.48 nm) and it can be seen that there is a good agreement between the experimental data and the theory close to the pH_{pzc}.
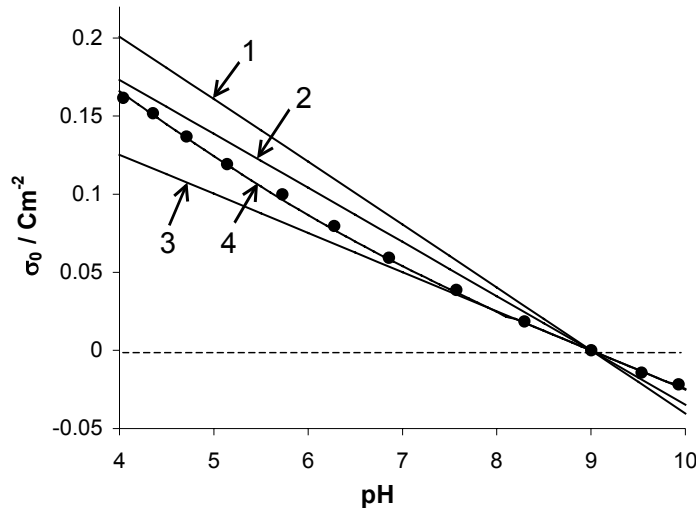

Figure 4.7   Model calculated surface charge curves in 0.1 M background electrolyte.
Curve 1: Point charges and no capacitor layer and no ion condensation; **Curve 2**: Finite ion size ($d = 0.425$ nm) but no capacitor layer or ion condensation **Curve 3**: $d = 0.425$ nm and capacitor layer ($w_c = 0.48$ nm) but no ion condensation. **Curve 4**: As curve 3 but ion condensation included. The points represent titrated surface charge of goethite in 0.1 M $NaClO_4$.

However, the linear response assumption in the CDH theory gives rise to a significant underestimation of the surface charge at pH values far away from the pH_{pzc}. The model prediction does not become satisfactory until we add a thin layer of condensed counter ions where nonlinear electrostatic response has been accounted for (curve 4 in Fig. 4.7). How this has been done will be described in the following section.

4.4.2 Inclusion of ion condensation

The linear response theory above is limited primarily in that it cannot account for cases where the electrostatic field acting upon the salt solution around the particle becomes so strong that the response is nonlinear. A good criterion for the maximal field tolerable in the linear response approximation is that the electrostatic energy experienced by an ion i in the field $\psi(r)$ equal $k_B T$ in magnitude, i.e.,

$$\left|\Psi(r)z_i e\right| = k_B T \tag{4.9}$$

A similar field criterion has been used before by, e.g., Schmitz [58]. The radius where this field criterion is satisfied will be denoted R_{ic} and it defines the outer boundary of a thin layer called an ion condensation (ic) layer, see Fig. 4.6. This is also the radius where the concentration of coions goes to zero in the linear response theory. In the ic-layer we will therefore only have counterions. Of course, the situation can occur when the field criterion never sets in and then there is no ic-layer at all. This will be the situation close to the pH_{pzc} where the surface charge is relatively low.

In this first implementation of the ion condensation presented in Paper VI the background electrolyte is assumed to be symmetrical so the field criterion is the same on both sides of pH_{pzc}. In addition, we have assumed that the charge density is constant within the ion condensation layer. Although this is a rather crude approximation it will be shown to produce very realistic results. The reason for this success is probably that the thickness of the ic-layer is very thin. It is often less than the diameter of an electrolyte ion. (Note that $w_{ic} = R_{ic} - R_c$, see Fig. 4.6.)

The calculation of the surface charge is slightly more complicated when the ion condensation is included. The reason for this is that before the chemical potential contribution from the ion condensation can be added to μ_{sc} in Eq. 4.8 the properties of the ic-layer has to be known. For example, for each salt concentration the thickness and the number of ions in the ic-layer must be determined as a function of particle charge. It is important to emphasise here that the parameters of the ic-layer are not working as fitting parameters in the model when the surface charge curve is calculated. Instead they are determined a priori from a minimization of the free energy. The details are given in Paper VI.

In Fig. 4.8 model calculated surface charge curves in 0.01, 0.1, and 1.0 M solutions is shown together with the experimental goethite data. The theory now includes the major mechanisms and a good description of the titrated surface charge is obtained. The ion condensation introduced accounts in a satisfactory way for the nonlinear electrostatic response.
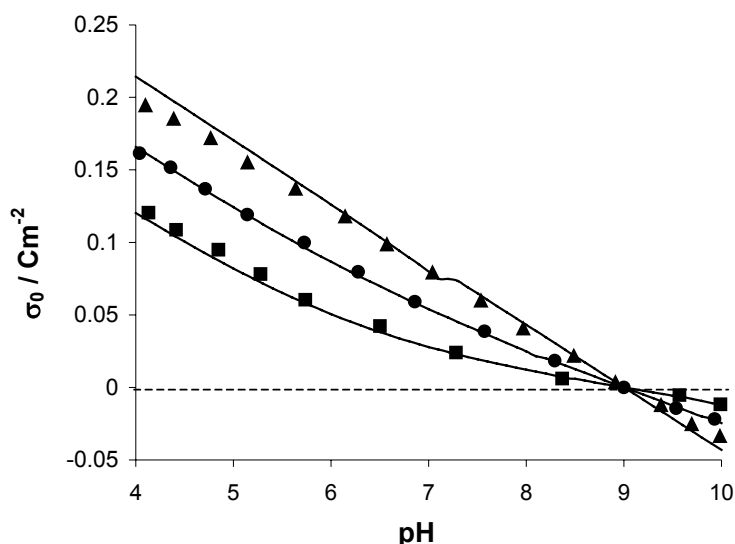

Figure 4.8   Results from the fit of titrated surface charge on goethite in 0.01 (■), 0.1(●), and 1.0 M (▲) NaClO$_4$ to the CDH model with ion condensation included. The fitted value of the capacitor layer thickness is 0.48 nm. The site density (6 per nm^2) was estimated from crystallographic considerations. Data from Paper VI.

The attentive reader may have noticed that there is a small plateau in the model curve in 1.0 M solution. It is located at the same pH-value as where the field criterion is satisfied. The plateau indicates that the onset of the ion condensation will in the beginning prevent the electrolyte ions from efficiently screening the charged particle. This yields a slightly lower surface charge than obtained with the purely linear response theory. The effect is also present at the lower salt concentrations but can hardly be seen in the plot of the surface charge curves.

At this stage the model is able to describe surface charge data of colloidal particles. However, it is likely that mechanisms corresponding to weak ion pairing of electrolyte ions, discussed in section 3.2.3, will be necessary for modelling surface charge data of some metal oxide/water interfaces. A major advantage of the CDH theory is its clear physical basis and its analytical mathematical form. This allows the results obtained to be assigned to physical mechanisms and conditions. From this point of view one may wonder whether the condensed ions may be attached to the particle following it as it moves, e.g., in the presence of an external electric field. At first sight, the boundary between the ion condensation layer and the diffuse CDH layer may seem to be a realistic location of the slip plane where the ζ-potential is measured. However, the

boundary condition implies that the electrostatic field at that plane will never exceed $k_B T/ze$. For a 1:1 electrolyte this corresponds to a potential of approximately 25 mV and that value is independent of background salt concentration. As we have seen in section 3.4 the zeta potentials of hematite particles are at least a factor of two higher. This is also the situation for goethite [59]. Therefore the slip plane must be located closer to the surface than the boundary between the ion condensation layer and the diffuse CDH layer. A detailed analysis of the relationship between the location of the slip plane and ion condensation in our present terminology is a suitable aim for future studies.

Another natural extension that is left for future work is to include also specific adsorption of other ions than protons. That will open up the field to handle chemical systems like those described in chapter 5 and 6 of this thesis.

Chapter 5

Cobalt sorption on hematite

Because of its relevance in natural water systems and in many industrial applications, a huge number of studies of metal ion sorption on different iron oxides exist in the literature. For a comprehensive review see for example Ref. [11]. Let us begin this section by pointing out some general features of metal sorption on oxide minerals [60]:

- Metal sorption increases sharply with *pH* because of the decreasing competition with protons for the surface ligand.
- The adsorption edge is displaced to lower *pH*-values with decreasing adsorbate-adsorbent ratios.
- Metal sorption is significant even below the *pH$_{pzc}$*. The surface is then positively charged when sorption commences, which means that the sorption of the positively charged ion takes place against an electrostatic repulsion.

In this work, we have chosen to study the sorption of cobalt(II) on hematite because of its relevance in the nuclear fuel process. ^{60}Co contributes to the build-up of radioactivity on fuel rods and in the water-cooling systems, and hematite is one of the many corrosion products present. In addition, both cobalt and hematite are present in the spent nuclear fuel that must be stored.

5.1 Radioactive tracer results

The sorption studies of cobalt(II) on hematite were performed on the larger particles, with diameter of ~0.6 μm, (Fig. 2.1 b). To be able to measure the protons involved in the cobalt sorption process with potentiometric titrations, the amount of cobalt has to be relatively high. This means a Co(II) concentration of the same order of magnitude as the concentration of active surface groups on the hematite surface. However, it is also important to study the sorption at much lower Co(II) concentrations. The radioactive tracer experiments were therefore performed both at the same Co(II) concentrations as used in the titrations (~$1 \cdot 10^{-4}$ M) and also at much lower concentrations (~$4 \cdot 10^{-8}$ M). The results are shown in Fig. 5.1.
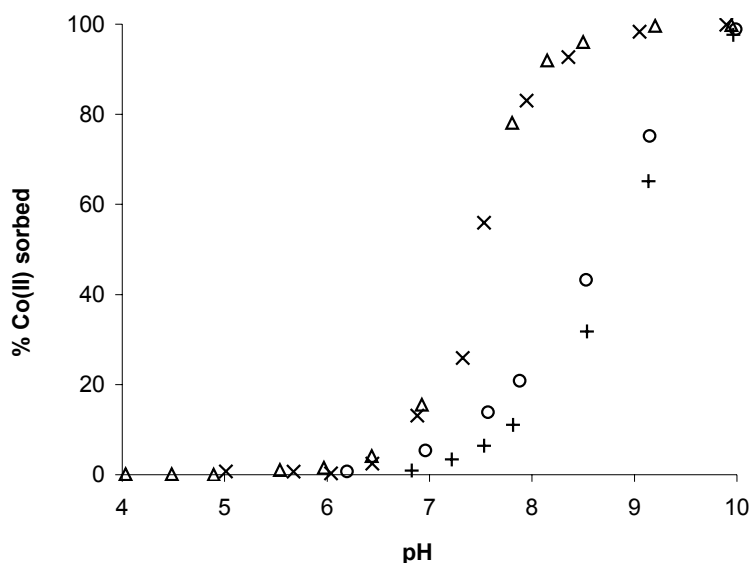
Figure 5.1   Sorption of Co(II) as a function of pH for different Co(II) concentrations and ionic strengths illustrated as percent sorbed of the total concentration. ($\times$) $[Co(II)]_{tot} = 4\cdot10^{-8}$ M and 0.05 M NaNO$_3$. (Δ) $[Co(II)]_{tot} = 4\cdot10^{-8}$ M and 1.0 M NaNO$_3$. (o) $[Co(II)]_{tot} = 0.9\cdot10^{-4}$ M and 0.1 M NaNO$_3$. (+) $[Co(II)]_{tot} = 1\cdot10^{-4}$ M and 1.0 M NaNO$_3$. Reprinted from Paper I.

It can be seen that the sorption takes place between pH 6.5 and 10 and as the concentration of cobalt is increased, the adsorption edge shifts to a higher pH-values. At low Co(II) concentrations the sorption is found to be independent of ionic strength. This is in good agreement with the results obtained by Kobal *et al*. [61]. However, at the higher Co(II) concentrations there is an indication of a weak ionic strength dependence.

5.2 Proton release during sorption of Co(II)

From potentiometric titrations, performed with and without Co(II) in the hematite suspension, protons involved in the sorption reactions of Co(II) on hematite could be extracted. The contribution from the hydrolysis of cobalt ions in the solution was accounted for by using equilibrium constants for the cobalt hydrolysis found in the literature [62]. To verify that no solid Co(OH)$_2$ was precipitated we used transmission FTIR. Withdrawn samples from titrations at pH 9 showed no solid Co(OH)$_2$ content.

By comparing the data from the radioactive tracer measurements and the proton data obtained by the potentiometric titrations, the number of protons released per cobalt sorbed was calculated as a function of pH. The results for Co(II) sorption in 0.1 M NaNO$_3$ solution are given in Fig. 5.2.
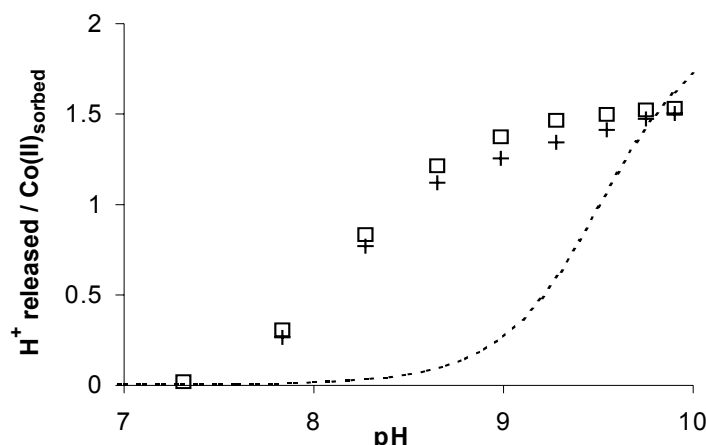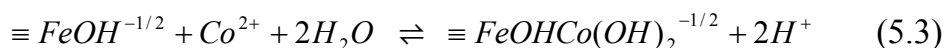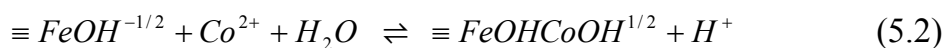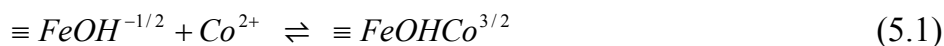
Figure 5.2   The number of protons released per Co(II) sorbed as a function of pH in 0.1 M NaNO$_3$. The dotted line represents the contribution of protons from the hydrolysis of Co(II), (□) represents data not corrected for the hydrolysis and (+) represents data corrected for the hydrolysis. Reprinted from Paper I.

It is clearly shown how the number of protons released increases from zero to approximately 1.5 between pH 7 and 9.5. This indicates that the sorption reaction does not involve the release of protons in the acid range, but when pH is increased, sorption reactions involving proton release dominate.

5.3 Modelling of Co(II) sorption

The experimental results presented above were modelled, using a 1-pK basic Stern model. The model parameters obtained from surface charge titrations on the same set of particles were used and kept fixed when the model for Co(II) sorption was constructed. Attempts were made to model the potentiometric titration data involving Co(II) in 0.1 M NaNO$_3$ solution with the following surface complexation reactions:

$$\equiv FeOH^{-1/2} + Co^{2+} \ \rightleftharpoons \ \equiv FeOHCo^{3/2} \tag{5.1}$$

$$\equiv FeOH^{-1/2} + Co^{2+} + H_2O \ \rightleftharpoons \ \equiv FeOHCoOH^{1/2} + H^+ \tag{5.2}$$

$$\equiv FeOH^{-1/2} + Co^{2+} + 2H_2O \ \rightleftharpoons \ \equiv FeOHCo(OH)_2^{-1/2} + 2H^+ \tag{5.3}$$

All cobalt complexes formed were put in the surface plane, i.e. an inner sphere complex formation was assumed. Since the experimental results show that the number of protons released ranges from zero to 1.5, a combination of at least two of these complexes was necessary.

To successfully describe the titration and sorption data it was necessary to introduce a low concentration of high affinity sites (0.1 sites per nm^2) for cobalt

sorption at the hematite surface. On these sites we allow the cobalt ions to adsorb without the release of protons, i.e. reaction 5.1. The most reasonable model was obtained if we, together with reaction 5.1 at the high affinity sites, allowed the cobalt to adsorb at both kinds of sites involving 2 H^+ release, i.e. reaction 5.3. With this model it was possible to describe the sorption in a very wide interval of cobalt concentration, ranging from 10^{-8} M to 10^{-4} M. The equilibrium constants for cobalt sorption are tabulated in Table 5.1

Table 5.1 Equilibrium constants obtained for cobalt sorption on hematite (298 K). The constants have been extrapolated down to zero ionic strength.

Surface complex	log K_i	Sites
$\equiv FeOHCo^{3/2}$	6.7	High affinity
$\equiv FeOHCo(OH)_2^{-1/2}$	-13.9	All sites

In Fig. 5.3 the calculated distribution diagrams at 0.1 M $NaNO_3$ are compared with experimental data from both titrations and sorption studies. For high Co(II) concentration ($1 \cdot 10^{-4}$ M), the high affinity sites will be saturated in the beginning of the pH region where adsorption takes place. As the pH increases the adsorption takes place at the other sites. When the Co(II) concentration is low ($4 \cdot 10^{-8}$ M), the adsorption will predominantly take place at the high affinity sites.
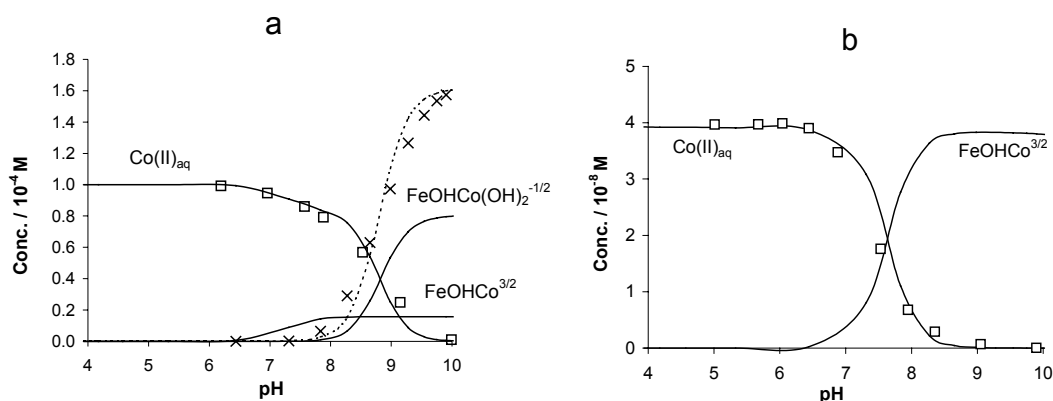

Figure 5. 3   Calculated distribution diagrams for the proposed model at 0.1 M $NaNO_3$ compared with excess proton data from titration ($\times$) and Co(II)$_{aq}$ concentrations from sorption experiments ($\square$), **a)** [Co(II)] = 0.1 mM and **b)** [Co(II)] = $4 \cdot 10^{-8}$ M. The dotted line in a) represents the model prediction of the concentration of protons emerging from the presence of Co(II). Reprinted from Paper I.

The proposed model was used in calculations at different ionic strengths but no significant ionic strength dependence could be established for the Co(II) sorption. The reason for this is that we did not use any outer-sphere surface complex for Co(II) in our model. Where outer-sphere complexes are introduced, much larger ionic strength dependence is normally found than was observed experimentally in this work [63].

In analogy to the model work for the surface charge data presented in section 3 we have tried to keep the number of parameters low and use quite a simple description of the processes taking place at the surface. Nevertheless, we believe that we have covered some main features of the sorption process of cobalt on hematite by combining sorption and titration experiments. The formation of the $\equiv FeOHCo(OH)_2^{-1/2}$ complex can be seen as a nonelectrostatic adsorption of the hydrolysed species $Co(OH)_2$. In the hydrolysis of Co(II), the first hydrolysed species $Co(OH)^+$ is of secondary importance. This is consistent with the observation made here that a reasonable model fit could be obtained without the presence of the surface species $\equiv FeOHCoOH^{1/2}$.

Of course, the physical reality is much more complicated than described in the proposed model. The trend in surface complexation modelling is towards model descriptions containing many different surface sites, species and planes of adsorption in the stagnant liquid layer. However, without additional reliable experimental data, the incorporation of such complications into the surface complexation model is questionable.

Chapter 6

Application to boiling water reactor data

As mentioned in the introduction a simplified version of the model for cobalt sorption has been used as a part of the interpretation of online radioactivity data from boiling water reactors (BWRs). Cobalt is of special interest since the activation product Co-60 contributes significantly to the radiation doses in BWRs during outage periods. The overall aim was to construct an activity build-up model that can be used in the future to simulate processes of corrosion, activation, cleanup, and deposition in the reactor. Previous models of this kind have not been able to simulate the effects of e.g. zinc injection, pH changes or hydrogen water chemistry in a scientifically sound manner. An important step in the activity build-up process that has not yet been accounted for is the formation of surface complexes on the oxide surfaces in the reactor water systems. Another important step is the diffusion of metal species within the oxide layers. Therefore, a model including these two mechanisms and various water phase equilibria has been developed.

The data used in the present application is extracted from radioactivity data for various nuclides taken from the reactor water but also from oxide layers inside pipes containing high temperature reactor water. The latter was collected using a mobile gamma spectroscopy equipment that is attached on the outside of the pipe of interest.

In this chapter, a short overview of the proposed mode will first be given. The submodel describing the complex formation at the oxide surface will then be treated in more detail. For a more comprehensive model description and detailed report of the results the reader is referred to the original project report [64].

6.1 Main model principles

The model for activity build-up is founded on three main processes, which are outlined in Fig. 6.1:

- Reaction in the water phase between dissolved species of corrosion products in the reactor water and precipitation of oxides. The oxides can deposit on system surfaces and/or the fuel cladding or form dispersions in the reactor water. The reactions are controlled by traditional chemical equilibria.

- Adsorption of dissolved species from the reactor water onto the oxide surfaces followed by formation of surface complexes. These processes are controlled by adsorption described in terms of surface complexation.
- Diffusion of metals through the oxides. The diffusion can take place both outward from the metal/oxide interface in a passivating oxide layer and inward from the adsorbed surface complex layer into the oxide. The diffusion rates are driven by the respective concentration gradients in the oxides. The rates are controlled according to traditional diffusion theory.
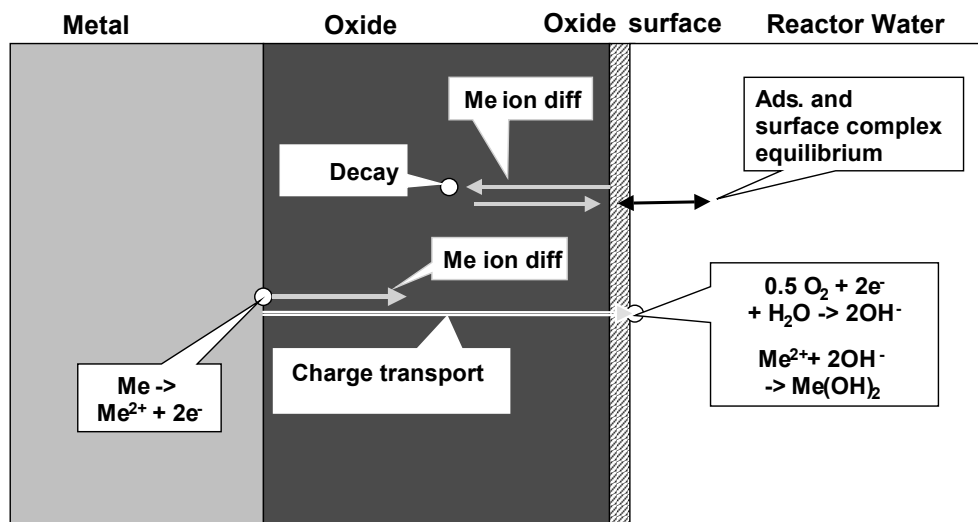
Figure 6.1   Schematic description of the proposed model for activity build-up in boiling water reactors. Picture reproduced from Ref. [64]

It was assumed that the diffusion of metal ions in the oxides is the rate-limiting process. Equilibrium could therefore be assumed for the surface complex formation at the oxide surface. One reaction step of special interest is the incorporation of surface complexes into the bulk oxide. It may be argued that this step is slow and could hence be rate-limiting. However, it was decided that this step should be handled as an integrated part of the diffusion. This implies that the transition from surface complex to oxide is controlled by traditional diffusion behaviour.

6.2 The surface complexation submodel

The basic Stern model (BSM) described in section 3.2.2 contains an inner Stern layer, which is necessary for the description of the screening of the charged particle at different background salt concentrations. However, in the reactor water the ionic strength is low, typically 10^{-6} M and therefore the BSM may be simplified to the diffuse layer model (DLM). This was verified by calculating the basic charging properties of hematite in 10^{-6} M ionic strength using the two models, Fig. 6.2. A site density of 10 $\equiv$FeOH$^{-1/2}$-groups per nm^2 was assumed. The difference between the calculated surface charge curves was small and will

not affect the modelling of metal ion sorption on the oxide surface. In this project the DLM is preferred over the BSM since it does not contain the capacitance, which introduces an additional fitting parameter.
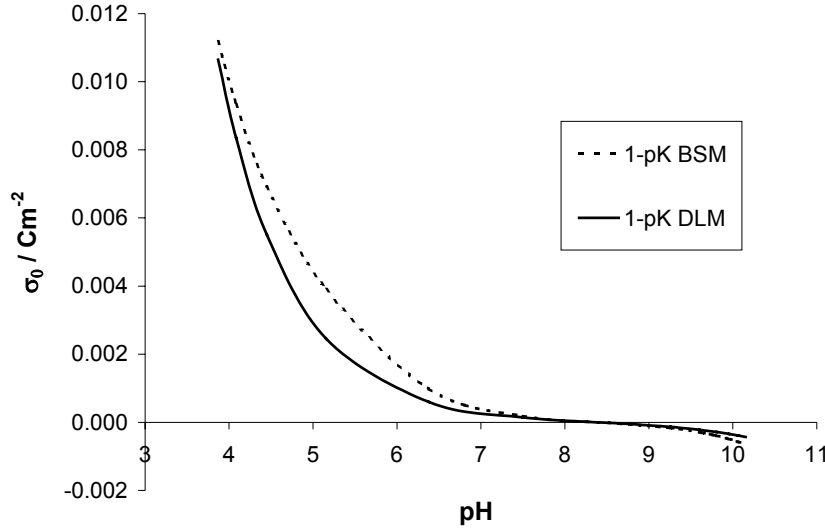

Figure 6.2   Calculated surface charge σ_0 of colloidal hematite in 10^{-6} M NaNO$_3$ using the 1-pK basic Stern model (BSM) and the 1-pK diffuse layer model (DLM).

A very simple surface complexation model based on the 1-pK DLM was then chosen for the present application. Only one type of surface complex formed was considered for each metal ion, here exemplified by the cobalt surface complex formation:

$$\equiv FeOH^{-1/2} + Co^{2+} \;\rightleftharpoons\; \equiv FeOHCo^{3/2} \tag{6.1}$$
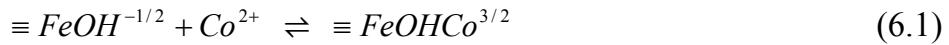
Since the intention was to find a model corresponding to the environment in the reactor some parameters have to be estimated from the conditions there. One such parameter that is important for the surface complexation calculations is the available oxide surface area per liter water. For a typical BWR the total surface area in the reactor is estimated to be 10 000 m^2 and the water volume is approximately 300 m^3, which yields an oxide surface area concentration of 0.033 m^2/liter. Another important parameter for the model is the point of zero charge pH_{pzc}, which is decreasing with temperature and for hematite at 300 °C the value 6.7 was used [65]. This means that at pH = 5.6 (neutral pH at the operating temperature in the reactor) the surface is slightly positively charged. Sorption of positively charged metal ions is still possible since specific chemical interactions are believed to dominate over the electrostatic effects. Also negative ions may adsorb on the surface but that has not been considered in this model so far.

The oxide layer present on different surfaces in the reactor is, of course, a mixture of many different oxides that may have quite different surface properties.

47

In addition there may be, on one single type of oxide, more than one kind of surface site. However, to keep the model simple and to avoid a large number of model parameters we will, in this first implementation of the model, make the assumption that the oxide can be represented by a single value of pH_{pzc} and that only one kind of surface site exists.

To perform the calculations of surface complexation equilibria the presented surface complexation model was added into the matrix of equilibria used for the water phase. The equilibrium calculations were performed with the code SOLGASWATER [66], version WinSGW 2.2. Surface reactions of Fe^{2+}, Ni^{2+}, Zn^{2+}, and Co^{2+} on the oxide surface were considered. From the equilibrium calculations of the soluble phase it was shown that both the non-hydrolyzed and different hydrolyzed complexes might be present in solution. It may therefore be argued that several surface reactions for each metal should be considered. That would yield too complicated a model with many fitting parameters and therefore the model was further simplified to account only for one surface reaction for each metal. A surface complex with the non-hydrolyzed metal ion was then chosen and the hydrolysis of the metal ions in the water phase was assumed inactive. The latter assumption may affect the formation of some solid phases in solution. This has to be examined further when the model shall be used to obtain quantitatively reliable results.

6.3 Model calculation results

To see if it was possible to obtain reasonable results with the chosen model, calculations were performed corresponding to both normal water chemistry (NWC) and hydrogen water chemistry (HWC) reactors. In Table 6.1 the metal ion concentrations in solution used for the calculations are tabulated. We have used approximate data from the reactor Barsebäck 2, which is a high zinc HWC reactor. In the NWC calculation the same metal ion concentrations were used except that the zinc concentration was set to zero. From the diffusion submodel an enrichment factor K_{enrich} was determined by comparing the concentration in the outer oxide layer with the measured reactor water concentration of the same nuclide. More explicitly K_{enrich} is defined as the concentration in the oxide divided by the concentration in the water, both expressed in mass percent. Typical values of K_{enrich} are included in Table 6.1. These values were used to estimate surface concentrations of the metal species. To be able to convert the surface concentration from the diffusion model (atoms/m^3 oxide) into the unit of adsorbed species per surface area an estimation of the thickness of the active surface layer of the oxide was necessary. The value 0.5 nm was chosen as estimated from inter atomic distances in the hematite structure.

Table 6.1 Values of metal ion concentrations used in the surface complexation calculations for Barsebäck 2. From the surface enrichment factor K_{enrich} surface concentrations were calculated for some metals.

Metal	Conc. in solution		typical K_{enrich}	Surface conc.		
	ppb	mM		mass%	mol / m^2	Atoms / nm^2
Fe(II)	2.0	3.6E-05	1.00E+07	2	5.93E-07	0.36
Ni(II)	0.5	8.5E-06	n.a.	-	-	-
Zn(II)	10.0	1.5E-04	1.00E+07	10	2.69E-06	1.62
Co(II)	0.05	8.5E-07	1.00E+07	0.05	1.46E-08	0.009

Note. n.a. = data not available

Already at this stage, before any surface complexation calculations have been performed, some interesting results can be noticed. The estimated concentration of zinc atoms on the surface is not very far from the estimated site density (10 nm^{-2}). It means that an effect due to the saturation of the sites with adsorbed zinc atoms is plausible. Note also that since the pH in solution is below the value of pH_{pzc} more than 50 % of the sites will be occupied with protons.

Attempts were then made to estimate values of some surface complexation constants. First a model calculation was performed corresponding to NWC (no zinc present). By using the same solution and surface concentrations for Co(II) as tabulated in Table 6.1 the equilibrium constant, log K_{Co} (reaction 6.1) was fitted and found to be approximately 7.1. In this calculation no other metal ions were assumed to form surface complexes. In the light of all approximations made in the model this value is surprisingly close to the constant found at 25 °C. To examine whether the adsorbed zinc atoms may prevent the cobalt from adsorbing the equilibrium constant for forming cobalt surface complex was kept fixed and used in an equilibrium calculation corresponding to high zinc, HWC conditions. The fitted surface complexation constant for zinc was then 6.7 and the amount of surface complex formed for cobalt then decreased by approximately 20 %. This is an indication of that the mechanism of site saturation is significant and can to some extent be described by surface complexation modelling.

It is important to emphasize that the results presented here are based on a first implementation of the activity build up model. In a continuation of this project further investigations will be performed so that more quantitatively reliable results can be obtained. For example, it will be interesting to examine:

- the effect of forming surface complexes also with the hydrolysed products of the metal ions in solution.
- the possibility of surface complex formation with negative ions, e.g. chromate ions.
- how the site density parameter is affecting the results of the model calculation.

However, already at this stage the results are very promising and the approach seems to be useful for the intended application. In addition, the project illustrates the usefulness of the surface complexation concept and its relevance in a real industrial problem.

Chapter 7

Concluding remarks

In the work presented in this thesis the concept of surface complexation has been used for interpreting various features of the iron oxide/water interface. For example the surface charge of suspended colloidal particles has been studied in detail as a function of pH and ionic strength. Hematite and goethite have been prepared and used as model substances in the experimental investigations. Colloidal hematite is a suitable model substance mainly because it is possible to obtain nearly spherical monodisperse particles of different sizes. This is extremely valuable since many of the underlying theories are developed assuming spherical particles of equal size. On the other hand, goethite particles have an acicular morphology with the length approximately ten times the width. The benefit of using these needle-like particles is that they often crystallize in a way so that very well defined limiting surface planes are developed. This will facilitate a crystallographic analysis of the surface and the ability to obtain the distribution of different types of surface groups (sites). However, from various model calculations performed in this work it can be concluded that a very reasonable approximation is to assume all active surface sites to have the same affinity for protons. This corresponds to a 1-pK model for the charging process and together with a basic Stern model for the liquid part of the electrical double layer it can be recommended as first choice surface complexation model. With this model most of the experimental data obtained in this work could be very well described.

Besides using existing surface complexation models a reformulation of the underlying theory of surface complexation has been performed using statistical mechanics. In this way a molecular description of surface complexation was obtained and with the new model it was possible to go one step beyond the equilibrium constants and the Gouy-Chapmann theory presently used in surface complexation. Besides the molecular description one of the main benefits of this new model approach is that it accounts for ion size effects in the screening atmosphere. In addition, we are not restricted to the planar surface limit; instead the more general case of a spherical particle of arbitrary size can be handled. A natural future extension is to use the theory also for other particle geometries. Another major advantage of the developed theory is its clear physical basis and its analytical mathematical form. This allows the results and the model parameters obtained to be assigned to physical mechanisms and conditions. For example, the surface site binding parameters in the model, i.e. the binding energy and the vibration frequency should be very closely related to the experimental data obtained from various spectroscopic techniques.

Although the foundation for a new surface complexation theory based on statistical mechanics has been set out it is necessary to incorporate a few more mechanisms before the model can serve as an attractive alternative to existing models. For example it is necessary to include also specific adsorption to surface sites of other ions than protons. It will then be possible to model more complex systems including specific adsorption of various ionic species. One such example is the cobalt sorption on hematite studied in this work.

Acknowledgements

References

1. Stumm, W., Huang, C.P., and Jenkins, S.R., Specific chemical interactions affecting the stability of dispersed systems. *Croatica Chem. Acta* **42,** 223 (1970).
2. Schindler, P.W. and Kamber, H.R., Die Acidität von Silanolgruppen. *Helv. Chim. Acta* **51,** 1781 (1968).
3. Schindler, P.W. and Gamsjäger, H., Acid-base reactions of the TiO_2 (Anatase)-water interface and the point of zero charge of TiO_2 suspensions. *Kolloid Z. Z. Polym.* **250,** 759 (1972).
4. Dzombak, D.A. and Morel, M.M., *Surface Complexation Modeling, Hydrous Ferric Oxide.* 1990, New York/Chichester/Brisbane/Toronto/Singapore: John Wiley & Sons.
5. Matijevic´, E. and Scheiner, P., Ferric hydrous oxide sols. III. Preparation of uniform particles by hydrolysis of Fe(III)-chloride, -nitrate, and -perchlorate solutions. *J. Colloid Interface Sci.* **63,** 509 (1978).
6. Matijevic´, E., Production of monodispersed colloidal particles. *Ann. Rev. Mater. Sci.* **15,** 483 (1985).
7. Atkinson, R.J., Posner, A.M., and Quirk, J.P., Adsorption of Potential-Determining Ions at the Ferric Oxide-Aqueous Electrolyte Interface. *J. Phys. Chem.* **71,** 550 (1967).
8. O´Brien, R.W., Electro-acoustic effects in a dilute suspension of spherical particles. *J. Fluid Mech.* **190,** 71 (1988).
9. O´Brien, R.W., Cannon, D.W., and Rowlands, W.N., Electroacoustic determination of particle size and zeta potential. *J. Colloid Interface Sci.* **173,** 406 (1995).
10. Ekberg, S., *Sorption Studies of Co onto Hematite.* Diploma work 1999, Department of Nuclear Chemistry, Göteborg, Sweden.
11. Cornell, R.M. and Schwertmann, U., *The Iron Oxides: Structure, Properties, Reactions, Occurence and Uses.* 1996, Weiheim, New York, Basel, Cambridge, Tokyo: VSH.
12. Hiemstra, T., van Riemsdijk, W.H., and Bolt, G.H., Multisite proton adsorption modeling at the solid /solution interface of (hydr)oxides: A new approach I. Model description and evaluation of intrinsic reaction constants. *J. Colloid Interface Sci.* **133,** 91 (1989).
13. Hiemstra, T., de Wit, J.C.M., and van Riemsdijk, W.H., Multisite proton adsorption modeling at the solid /solution interface of (hydr)oxides: A new approach II. Application to various oímportant (hydr)oxides. *J. Colloid Interface Sci.* **133,** 105 (1989).
14. Hohl, H. and Stumm, W., Interactions of Pb 2+ with hydrous alfa-Al2O3. *J. Colloid Interface Sci.* **55,** 281 (1976).
15. Bolt, G.H. and van Riemsdijk, W.H., in *Soil Chemistry, B. Physio-Chemical Models*, G.H. Bolt, Editor. 1982, Elsevier: Amsterdam. p. Ch 13.
16. van Riemsdijk, W.H., Bolt, G.H., Koopal, L.K., and Blaakmeer, J., Electrolyte Adsorption on Heterogeneous Surfaces: Adsorption Models. *J. Colloid Interface Sci.* **109,** 219 (1986).
17. Borkovec, M., Origin of 1-pK and 2-pK Models for Ionizable Water-Solid Interfaces. *Langmuir* **13,** 2608 (1997).
18. Westall, J. and Hohl, H., A Comparison of Electrostatic Models for the Oxide/Solution Interface. *Advances in Colloid and Interface Science* **12,** 265 (1980).
19. Boily, J.F., *The Surface Complexation of Ions at the Goethite (α-FeOOH)/Water Interface: A Multisite Complexation Approach,* Thesis 1999, Umeå University, Sweden.
20. Venema, P., Hiemstra, T., and van Riemsdijk, W.H., Comparison of Different Site Binding Models for Cation Sorption: Description of pH Dependency, Salt Dependency, and Cation-Proton Exchange. *J. Colloid Interface Sci.* **181,** 45 (1996).
21. Gouy, G., *J. Phys. Rudium* **9,** 457 (1910).
22. Chapman, D.L., *Philos. Mag.* **25,** 457 (1913).
23. Sposito, G., On the Surface Complexation Model of the Oxide-Aqueous Solution Interface. *J. Colloid Interface Sci.* **91,** 329 (1983).

24. Stern, O., *Z. Elektrochem.* **30,** 508 (1924).
25. Grahame, D.C., *Chem. Rev.* **47,** 441 (1947).
26. Parsons, R. and Zobel, R., The Interface Between Mercury and Aqueous Sodium Dihydrogen Phosphate. *J. Electroanal. Chem.* **9,** 333 (1965).
27. Siviglia, P., Daghetti, A., and Trasatti, S., Influence of the preparation temperature of ruthenium dioxide on its point of zero charge. *Colloids and Surfaces* **7,** 15 (1983).
28. Gibb, A.W.M. and Koopal, L.K., Electrochemistry of a Model for Patchwise Heterogeneous Surfaces: The Rutile-Hematite System. *J. Colloid Interface Sci.* **134,** 122 (1990).
29. Koopal, L.K., Ion adsorption on mineral oxides surfaces, in *Adsorption on New and Modified Inorganic Sorbents*, A. Dabrowski and V.A. Tertykh, Editors. 1996, Elsiever ScienceB.V. p. 757.
30. Hiemstra, T. and van Riemsdijk, W.H., Physical chemical interpretation of primary charging behaviour of metal (hydr)oxides. *Colloids and Surfaces* **59,** 7 (1991).
31. Lützenkirchen, J., Boily, J.F., Lövgren, L., and Sjöberg, S., Limitations of the potentiometric technique in determining the proton active site density of goethite surfaces. *Geochim. Cosmochim. Acta* **66,** 3389 (2002).
32. Lützenkirchen, J., Comparison of 1-pK and 2-pK Versions of Surface Complexation Theory by Godness of Fit in Describing Surface Charge Data of (Hydr)oxides. *Environ. Sci. Technol.* **32,** 3149 (1998).
33. Rietra, R.P.J.J., Hiemstra, T., and van Riemsdijk, W., H., Electrolyte Anion Affinity and Its Effect on Oxyanion Adsorption on Goethite. *J. Colloid Interface Sci.* **229,** 199 (2000).
34. Schudel, M., Behrens, S.H., Holthoff, H., Kretzschmar, R., and Borkovec, M., Absolute Aggregation Rate Constants of Hematite Particles in Aqueous Suspensions: A Comparison of Two Different Surface Morphologies. *J. Colloid Interface Sci.* **196,** 241 (1997).
35. Lyklema, J., *Fundamentals of Interface and Colloid Science.* 1995, San Diego: Academic Press.
36. Hunter, R.J., *Foundations of Colloid Science, 2nd ed.* 2001, Oxford: Clarendon Press.
37. von Smoluchowski, M., *Z. Physik. Chem.* **92,** (1918).
38. O´Brien, R.W. and White, L.R., Electrophoretic Mobility of a Spherical Colloidal Particle. *J. Chem. Soc. Faraday Trans. 2* **74,** 1607 (1978).
39. Hunter, R.J., *A User's Guide to the AcoustoSizer*, Colloidal Dynamics Pty Ltd.
40. Mangelsdorf, C.S. and White, L.R., Electrophoretic Mobility of a Spherical Colloidal Particle in an Oscillating Electric Field. *J. Chem. Soc. Faraday Trans.* **88,** 3567 (1992).
41. O´Brien, R.W., The Dynamic Mobility of a Porous Particle. *J. Colloid Interface Sci.* **171,** 495 (1995).
42. Kijlstra, J., van Leeuwen, H.P., and Lyklema, J., Low-frequency dielectric relaxation of hematite and silica sols. *Langmuir* **9,** 1625 (1993).
43. Shubin, V.E., Hunter, R.J., and O´Brien, R.W., Electroacoustic and Dielectric Study of Surface Conduction. *J. Colloid Interface Sci.* **159,** 174 (1993).
44. Mangelsdorf, C.S. and White, L.R., Effects of Stern-layer Conductance on Electrokinetic Transport Properties of Colloidal Particles. *J. Chem. Soc. Faraday Trans.* **86,** 2859 (1990).
45. Mangelsdorf, C.S. and White, L.R., The dynamic double layer - Part 1 - Theory of mobile Stern layer. *J. Chem. Soc. Faraday Trans.* **94,** 2441 (1998).
46. Mangelsdorf, C.S. and White, L.R., The dynamic double layer - Part 2 - Effects of Stern layer conduction on the high-frequency electrokinetic transport properties. *J. Chem. Soc. Faraday Trans.* **94,** 2583 (1998).
47. Charmas, R., Piasecki, W., and Rudzinski, W., Four Layer Complexation Model for Ion Adsorption Electrolyte/Oxide Interface: Theoretical Foundations. *Langmuir* **11,** 3199 (1995).
48. Nordholm, S. and Haymet, A.D.J., Generlized van der Waals Theory. I Basic Formulation and Application to Uniform Fluids. *Aust. J. Chem.* **33,** 2013 (1980).
49. Nordholm, S. and Penfold, R., The GvdW Theory: A Density Functional Theory of Adsorption, Surface Tension, and Screening, in *Liquid Interfaces in Chemical, Biological,*

and Pharmaceutical Applications, A.G. Volkov, Editor. 2000, Marcel Dekker, Inc.: New York, Basel. p. 83.

50. Nordholm, S., Generlized van der Waals Theory. XII Application to Ionic Solutions. *Aust. J. Chem.* **37,** 1 (1984).

51. Debye, P. and Hückel, H., *Physik. Z.* **24,** 185 (1923).

52. Debye, P. and Hückel, H., *Physik. Z.* **25,** 97 (1924).

53. Van Megen, W. and Snook, I.K., *Mol. Phys.* **39,** 1043 (1980).

54. Robinson, R.A. and Stokes, R.H., *Electrolyte Solutions*. 1970, Butterworth, Stoneham: MA.

55. Abbas, Z. Private communication.

56. Abbas, Z., Gunnarsson, M., Ahlberg, E., and Nordholm, S., Corrected Debye-Hückel Theory of Salt Solutions - Size Asymmetry and Effective Diameters. *J. Phys. Chem. B* **106,** 1403 (2002).

57. Fokkink, L.G.J., de Keizer, A., and Lyklema, J., Temperature Dependence of the Electrical Double Layer on Oxides: Rutile and Hematite. *J. Colloid Interface Sci.* **127,** 116 (1989).

58. Schmitz, K.S., Effective Screened Coulomb Charge of Spherical Colloidal Particles. *Langmuir* **16,** 2115 (2000).

59. Boily, J.F., Lützenkirchen, J., Balmès, O., Beattie, J., and Sjöberg, S., Modeling proton binding at the goethite (α-FeOOH)-water interface. *Colloids and Surfaces A* **179,** 11 (2001).

60. Morel, F.M.M. and Hering, J.G., *Principles and Applications of Aquatic Chemistry*. 1993, New York/Chichester/Brisbane/Toronto/Singapore: John Wiley & Sons.

61. Kobal, I., Hesleitner, P., and Matijevic´, E., Adsorption at solid/solution interfaces. 6. Interactions of Co 2+ ions with spherical hematite particles. *Colloids and Surfaces* **33,** 167 (1988).

62. Baes, C.F. and Mesmer, R.E., *The Hydrolysis of Cations*. 1986, New York: John Wiley and Sons Inc.

63. Hayes, K.F. and Leckie, J.O., Modeling ionic strength effects on cation adsorption at hydrous oxide/solution interfaces. *J. Colloid Interface Sci.* **115,** 564 (1987).

64. Lundgren, K., Kelén, T., Gunnarsson, M., and Ahlberg, E., *A new model for activity buildup in BWRs adopting theories for surface complexes and diffusion in oxide layers*. 2001, SSI.

65. Schoonen, M.A.A., Calculation of the point of zero charge of metal oxides between 0 and 350 C. *Geochim. Cosmochim. Acta* **58,** 2845 (1994).

66. Eriksson, G., An Algorithm for the Computation of Aqueous Multicomponent, Multiphase Equilibria. *Analytica Chimica Acta* **112,** 375 (1979).